

AMERICAN UNIVERSITY OF BEIRUT

THERMAL CREEP EFFECT ON THE BEHAVIOR OF FLUSH
END-PLATE CONNECTION UNDER PROLONGED
TRANSIENT HEATING CONDITIONS

by
FARAH MOUNIR AL MOHTAR

A thesis
submitted in partial fulfillment of the requirements
for the degree of Master of Engineering
to the Department of Civil and Environmental Engineering
of the Maroun Semaan Faculty of Engineering and Architecture
at the American University of Beirut

Beirut, Lebanon
January 2020


AMERICAN UNIVERSITY OF BEIRUT

THERMAL CREEP EFFECT ON THE BEHAVIOR OF FLUSH
END-PLATE CONNECTION UNDER PROLONGED
TRANSIENT HEATING CONDITIONS


by
FARAH MOUNIR AL MOHTAR

Approved by:

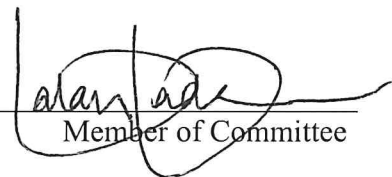
Dr. Elie G. Hantouche, Associate Professor
Department of Civil and Environmental Engineering


Advisor

Dr. Mayssa Dabaghi, Assistant Professor
Department of Civil and Environmental Engineering


Member of Committee

Dr. Salah Sadek, Associate Dean and Professor
Department of Civil and Environmental Engineering


Member of Committee

Date of thesis defense: January 23, 2020

AMERICAN UNIVERSITY OF BEIRUT

THESIS, DISSERTATION, PROJECT RELEASE FORM

Student Name: AL Mohtar Farah Mounir
Last First Middle

Master's Thesis Master's Project Doctoral Dissertation

I authorize the American University of Beirut to: (a) reproduce hard or electronic copies of my thesis, dissertation, or project; (b) include such copies in the archives and digital repositories of the University; and (c) make freely available such copies to third parties for research or educational purposes.

I authorize the American University of Beirut, to: (a) reproduce hard or electronic copies of it; (b) include such copies in the archives and digital repositories of the University; and (c) make freely available such copies to third parties for research or educational purposes after:

One ---- year from the date of submission of my thesis, dissertation, or project.
Two ---- years from the date of submission of my thesis, dissertation, or project.
Three 3 years from the date of submission of my thesis, dissertation, or project.

Farah AL Mohtar Feb. 3. 2020
Signature Date

ACKNOWLEDGMENTS

I would like to thank my advisor Dr. Elie Hantouche for his support, patience, and guidance during my study. I appreciate his dedication and enthusiasm for the development of this research work. His expertise and valuable critics helped me develop my research skills, and knowledge throughout the time spent at the American University of Beirut.

My recognition and gratitude are also extended to my committee Dr. Mayssa Dabaghi and Dr. Salah Sadek.

Furthermore, I would like to acknowledge the financial support provided by the American University of Beirut Research Board under Award No. 103604.

The continuous encouragement and support from my family and friends will always be remembered. Thank you.

AN ABSTRACT OF THE THESIS OF

Farah Mounir Al Mohtar for Master of Engineering
Major: Civil and Environmental Engineering

Title: Thermal Creep Effect on the Behavior of Flush End-Plate Connection under Prolonged Transient Heating Conditions

The properties of steel material become dependent on the temperature and duration of heating during a fire event. Thermal creep strain of steel is a time-dependent inelastic deformation that becomes significant under constant load and high temperatures. The goal of this study is to understand the thermal creep effect on the behavior of beam-to-column flush end-plate connections subjected to transient fire conditions.

Finite element (FE) models were developed and validated against experimental work available in the literature. FE parametric studies were conducted to study the overall response of the connection with and without the explicit consideration of thermal creep. The parameters include: heating/cooling rate, beam length, load ratio, plate thickness, bolt size, and thermal creep effect in bolts.

A mechanical model was developed to predict the flush end-plate connection behavior subjected to fire temperatures. The proposed model is based on geometrical components and material properties of the connection. This model is able to predict the thermal beam axial forces including the effect of beam mid-span deflection. The proposed model is also able to predict the time-dependent behavior of the flush end-plate connection where thermal creep strains are incorporated in slow heating rates.

This work shows the importance the including the effect of thermal creep strains in designing flush end-plate connections subjected to prolonged heating conditions.

CONTENTS

ACKNOWLEDGMENTS	I
AN ABSTRACT OF THE THESIS OF.....	II
ILLUSTRATIONS	V
TABLES	VII
ABBREVIATIONS	VIII
Chapter	
I. INTRODUCTION.....	12
II. THERMALCREEP STRAINS.....	17
A. Thermal Creep Strains of Structural Steel	17
B. Thermal Creep Strains of Bolts.....	18
III. FE MODEL OF FLUSH END-PLATE CONNECTION.....	21
A. Flush End-plate Connection Assemblies	21
1. Experimental Data Set.....	22
2. Material Properties	23
B. Description of the FE Model.....	24
1. FE Model Discretization	24
2. Boundary Conditions.....	25
3. Analysis Procedure.....	26
C. Model Validation	27
D. Description of the Thermal Creep Model	31
IV. PARAMETRIC STUDIES.....	33
A. Heating/Cooling rate.....	33
B. Beam Length	35

C. Load Ratio.....	37
D. Creep Effect in Bolts.....	38
E. Flush End-Plate Thickness and Bolt Size	40
V. MECHANICAL MODEL	43
A. Component Stiffness.....	44
1. Column Web in Tension	44
2. Column Web in Shear	44
3. Column Flange in Bending	45
4. Flush End-Plate in Bending.....	45
5. Tension Bolts.....	45
6. Unheated Column.....	46
B. Equivalent Connection Stiffness	46
C. Beam Axial Force	47
1. Fast Analysis	47
2. Thermal Creep Analysis.....	48
D. Flush End-plate Connection Limit State.....	50
E. Beam Mid-span Deflection	51
F. Model Performance	54
VI. SUMMARY, CONCLUSIONS AND RECOMMENDATIONS	60
A. Summary and conclusions	60
B. Recommendations.....	62
BIBLIOGRAPHY	64
APPENDIX	67

ILLUSTRATIONS

Figure		Page
1.	Stages of thermal creep strains.....	6
2.	Flush end-plate connection experimental setup by Wang et al. (2011)..	11
3.	Dimensions of the proposed flush end-plate connection.....	12
4.	Flush end-plate connection modeling details.....	14
5.	Comparison between the beam axial force of the experiment and the FE models with and without creep: (a) Test-3; (b) Test-8.....	18
6.	Comparison between the beam mid-span deflection of the experiment and the FE models with and without creep: (a) Test-3; (b) Test-8.....	19
7.	Comparison between the deformed flush end-plate connection of the experiment (Wang et al., 2011) and the FE models: (a) Test-3; (b) Test-8.....	20
8.	The effect of different heating and cooling rates on the flush end-plate connection behavior: (a) beam axial force; (b) beam mid-span deflection.	23
9.	The effect of beam length on the flush end-plate connection behavior: (a) beam axial force; (b) beam mid-span deflection.....	25
10.	The effect of load ratio on the flush end-plate connection behavior: (a) beam axial force; (b) beam mid-span deflection.....	27
11.	The effect of creep in bolts on the flush end-plate connection behavior: (a) beam axial force; (b) beam mid-span deflection.....	28
12.	The effect of plate thickness on the flush end-plate connection behavior: (a) beam axial force; (b) beam mid-span deflection.....	29
13.	The effect of bolts size on the flush end-plate connection behavior: (a) beam axial force; (b) beam mid-span deflection.....	30
14.	Components of the flush end-plate connection in fire.....	32

15.	Mechanical model results on the heating/cooling rate parameter with and without creep; (a) Fast rate and 20deg/min; (b) 5deg/min; (c) 2.5deg/min.....	44
16.	Mechanical model results on the beam length parameter with and without creep; (a) 1L; (b) 1.25L; (c) 1.5L.....	46
17.	Mechanical model results on the load ratio parameter with and without creep; (a) 50%; (b) 70%; (c) 90%.....	47

TABLES

Table		Page
1.	Bolt creep constants based on steady-state heating conditions (Matar, 2014).....	8
2.	Bolt creep constants representing transient heating conditions.....	8
3.	Summary of the section and material properties used in FE models...	13
4.	The temperature profiles of the FE validation models.....	16
5.	Beam mid-span deflection of all parameters subjected to fast heating.....	41
6.	Beam mid-span deflection of all parameters subjected to heating while considering the effect of thermal creep; (a) heating phase, (b) cooling phase.....	41

ABBREVIATIONS

a, b, c	material temperature-dependent constants used in Fields and Fields (1988)
A_b	beam cross-sectional area contributing to the beam axial force
A_{vc}	web shear area of a column
$b_{eff,cw}$	effective width of a column web
b_p	width of the end-plate
C_1, C_2, C_3, C_4	constants for steady-state heating by Matar (2014)
d_{cw}	effective depth of a column web
d_b	bolt diameter
e	distance between bolt centerline and the edge of the flush-endplate
E_b	beam elastic modulus
E_{bolt}	bolts elastic modulus
E_c	column elastic modulus
$E_{c,u}$	column elastic modulus at ambient
E_p	end-plate elastic modulus
f_{py}	yield strength of the end-plate material
g	center to center distance between the bolts in a bolt row
h_c	height of a column's cross-section
h_1	distance from the lower beam flange to the center of the first bolt row
I_b	moment of inertia of the beam

I_{bolt}	moment of inertia of the bolts
I_c	moment of inertia of the column across its major axis
K	equivalent connection stiffness
$K_{b,t}$	bolt stiffness in tension
$K_{cf,b}$	column flange stiffness in bending
$K_{c,u}$	unheated column section stiffness
$K_{cw,s}$	column web stiffness in shear
$K_{cw,t}$	column web stiffness in tension
$K_{p,b}$	end-plate stiffness in bending
K_1, K_2, K_3	stiffness used in calculating the equivalent connection stiffness
$l_{eff,cf}$	effective length of a column flange
$l_{eff,pb}$	effective length of the end-plate
L_b	is the beam length
L_{bolt}	bolt shank length
$L_{c,u}$	unheated column section length
LR	load ratio
m	distance between fillet weld and bolt centerline
M_n	moment nominal capacity of the end-plate in bending
N	constant used for creep in cooling
P_f	distance between the center of the first bolt row and the lower end of the beam top flange
$P - \Delta$	P-delta effect caused by fast heating rates

$P - \Delta_c$	P-delta effect caused by slow rates
P_c	beam axial force under slow heating rates
P_{fast}	beam axial force under fast heating rates
P_i	summation of generated axial force
$P_{(i-1)}$	generated beam axial force in a step before
R	heating/cooling rate
s	is a constant for end-plate yielding
t	time
t_{cf}	column flange thickness
t_{cw}	column web thickness
t_p	end-plate thickness
T	temperature
y	location of the neutral axis
Y	constant for end-plate yielding
z	lever arm distance
α	coefficient of thermal expansion
β	transformation parameter
ΔP_i	incremental beam axial force
ΔT	incremental change in temperature
$\Delta \varepsilon_c$	thermal creep strain difference per iteration
ε_c	thermal creep time-dependent strain

ν	<i>Poisson's ratio</i>
δ	beam mid-span deflection due to fast heating rates
δ_c	beam mid-span deflection due to slow heating rates
σ	stress
σ_{fast}	stress under fast heating conditions
σ_c	stress under slow heating conditions
$(\sigma_c)_{cooling}$	stress under slow heating conditions in the cooling phase
$(\sigma_c)_T$	stress under slow heating conditions in the cooling phase at each temperature
$(\sigma_c)_{600^\circ C}$	stress under slow heating conditions at 600°C
σ_M	stress due to $P - \Delta_c$ under slow heating rates
σ_x	stress along the x-direction
σ_y	stress along the y-direction
σ_z	stress along the z-direction

Special Symbols

Δ	prefixed to other term denotes an increment or change
$\frac{\partial}{\partial x}$	denotes partial differentiation with respect to x

CHAPTER I

INTRODUCTION

Structural steel is commonly used in the construction of high rise buildings due to its mechanical properties and ease of construction. These structures are susceptible to fire disasters where the rapid loss of strength and stiffness in addition to high thermal conductivity of steel impose a threat on its safety. Thus, steel structures should be appropriately designed to ensure structural fire safety.

In steel frames, a connection transfers the load from a beam to a column and ensures the stability of the structure. At ambient temperatures, connections are either designed as ideally pinned or fixed. As considered by designers, pinned connections allow the rotation of the connection without the transfer of any bending moment between the connected members. On the other hand, fixed connections are designed to fully transfer the bending moment and restrain connection rotations. However, during a fire incident, the analysis of the behavior of a steel structure becomes more complex. In a beam-column connection, the thermal induced compressive forces are generated due to the expansion of the beam and axial restraint of the column. At later stages of heating, the beam's behavior changes from flexure to combined flexure and tension known as catenary action. Thus, the generated forces in the beam change from compressive to tensile. This is accompanied by an increase in the beam's deflection when the beam reaches its load bearing capacity. This sagging of the beam at the end stages of the fire generates large rotational demands. The beam tensile forces continue to increase during the cooling phase (Yu and Liew, 2005).

Many models were proposed based on the concept of retention factors at specific temperatures to capture the change in the mechanical properties of steel (Eurocode 3-1.2, 2005, Poh, 2001, Lie, 1992). When the temperature of the steel reaches around one-third of its melting point, the material behavior is influenced by the thermal creep strains (Kodur et al., 2010). To quantify the thermal creep strains, creep tests are conducted by subjecting the steel material to constant load and temperature for a period of time. The creep of steel is incorporated into finite element models in two methods: implicit or explicit. Eurocode 3-1.2 (2005) has partially included the effect of these strains implicitly in the stress-strain curves. This implicit inclusion of creep in *Eurocode 3* is considered conservative when steel is subjected to heating rates lower than 10°C/min (Toric et al., 2016). Kodur et al. (2010) included thermal creep in the analysis of simply supported beams using *Eurocode 3* material properties. The results showed an overestimation of the beam-mid span deflection when compared to experimental data. Explicit consideration of creep is based on utilizing a defined creep equation to calculate the change in creep strain at each iteration. Explicit creep can be incorporated in finite element models in the form of user-defined subroutines. Models were proposed for a wide range of materials Q460 high-strength steel, ASTM A992, ASTM A36, and ASTM A325 bolts (Wang et al., 2016, Morovat, 2014, Fields and Fields, 1988, Matar, 2014), respectively. Hantouche et al. (2018) and Al Haddad et al. (2019) developed subroutines based on *Fields and Fields* creep model for the materials S275 and S355, respectively. The authors incorporated these models in the FE analysis of shear tab and shear end-plate connections in fire.

Recently, researchers have recognized the significance of thermal creep effect on structures (Kodur and Dwaikat, 2010, Morovat, 2014). In concentrically loaded

columns subjected to fire, the effect of creep on the column buckling depends on its slenderness, load duration, and temperature (Morovat, 2014). Kodur and Dwaikat (2010) compared the behavior of restrained beams using two widely used creep models: *Eurocode* and *Harmathy* creep models. The results show that ignoring the creep strains in the analysis of restrained beams can lead to an overestimation of the beam axial force.

Research concerning the behavior of connections in fire is crucial after the investigation of the collapse of the World Trade Center 7 on 9/11 that was possibly due to the failure of a connection (NIST, 2008). Flush end-plate connections are popular due to their feasibility and simple detailing, welded in the workshop and bolted on site. These connections are typically designed to withstand shear and moment. Flush end-plate connections are known to maintain high performance, ductility, and strength in seismic areas due to their efficient energy dissipation. Several researchers studied the behavior of an isolated connection experimentally and numerically without considering the effect of creep (Silva Da et al., 2005, Al-Jabri et al., 2006, Qiang et al., 2013, Yu et al., 2011). Clearly, the flush end-plate connection loses its strength and moment resistance capacity at elevated temperatures. The moment and force rotation curves of flush end-plate connections were plotted while the thermal beam axial force was ignored. Recently, the effect of thermal creep was included in the analysis of an isolated flush end-plate connection (Morovat et al., 2018). The authors investigated the connection subjected to shear and tension under steady-state conditions. The effect of creep on the strength and rotational capacity of the connection was presented in the form of force-rotation isochronous curves. The isochronous curves relate the connection rotation and the total force at each point in time. However, no numerical analysis has so

far focused on the explicit thermal creep effect of a beam-column connection subjected to transient heating conditions.

Mechanical models or component-based models are being recently developed by researches because of their accuracy, time competency, and low cost. Del Savio et al. (2009) proposed a generalized component-based model that predicts the bending moment-rotation curves of end-plate connections. The implementation of this generalized model was validated against six experiments of extended end-plate connections subjected to axial forces and bending moments. Silva Da et al. (2005) developed a component model composed of springs and rigid links of a flush end-plate connection in fire. The moment-rotation curves at steady-state temperatures were presented and compared with experimental tests. El Ghor and Hantouche (2017) developed a mechanical-based model of an isolated flush end-plate connection. This model did not account for the effect of the column restraint, and thus the generated beam axial force. A *Modified Burgers* model was used to estimate the time-dependent behavior of the connection in steady-state heating conditions. Other researchers integrated the component-method with finite element analysis. This approach consists of developing a component-based model for the end-plate member and incorporating it in *Vulcan* software while ignoring the creep strains of steel at elevated temperatures (Al-Jabri, 2004, Block et al., 2007, Dong et al., 2015). (Al-Jabri, 2004, Block et al., 2007, Dong et al., 2015). Previous research work has focused on developing mechanical models for end-plate connections that predict the moment-rotation curves at ambient and elevated temperatures. However, limited work was done to develop a mechanical model of the full-scale connection under transient heating conditions with the inclusion of thermal creep strains.

To address this shortcoming in the literature, the time-dependent response of a beam-column flush end-plate under transient heating is investigated using finite element analysis then a mechanical model is developed. FE models are developed in ABAQUS and validated against experimental work performed by Wang et al. (2011). Thermal creep models are developed by incorporating a transient creep user-developed subroutine. Also, parametric studies are conducted to highlight the parameters that affect the behavior of the connection with and without creep. The parameters are the heating/cooling rate, beam length, load ratio, plate thickness, bolt size, and creep effect in bolts. The results of the simulations are presented and discussed to demonstrate the effect of thermal creep strains on the flush end-plate connection. Using the results of the FE models and the parametric studies, the components of the flush end-plate are identified. A mechanical model is developed from these components to predict the generated beam axial force while accounting for the high beam mid-span deflection. This model is able to predict the behavior of a beam-column flush end-plate connection under fast and prolonged heating conditions.

CHAPTER II

THERMAL CREEP STRAINS

A. Thermal Creep Strains of Structural Steel

The thermal creep strains are defined as the time-dependent deformation under high stresses at elevated temperatures. At high temperatures, creep strains can be developed at stresses lower than the yielding stress of steel. Steady-state tensile coupon tests are performed to study the creep phenomena where steel is subjected to high temperature and applied mechanical load for a long period of time. Creep curves are plotted with respect to time and can be divided into three stages as shown in Figure. 1.

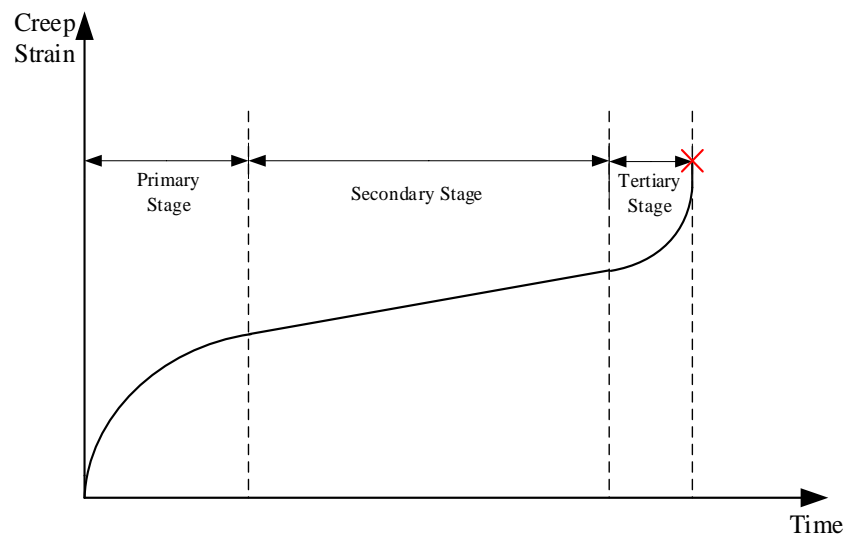


Figure. 1. Stages of thermal creep strains

The primary stage of the creep curve starts at a rapid creep strain rate and decreases with time. The secondary stage, known as the steady-state phase, is characterized by a

constant creep strain rate. In the tertiary stage, this rate increases until a fracture occurs due to the necking of the cross-section (Hantouche et al., 2018).

The creep model of A36 steel proposed by Fields and Fields (1988) predicts the thermal creep effect between temperatures 350°C to 600°C and up to 6% strain rate. This model adopts a power-law representation to predict the primary and secondary thermal creep strains. The equation can be written as:

$$\varepsilon_c = at^b \sigma^c \quad (1)$$

Where t = time (minute), σ = stress (MPa), ε_c = creep strain (unitless), and a , b and c are temperature-dependent material parameters.

In this study, the thermal creep of steel is explicitly incorporated as a user-defined subroutine based on *Fields and Fields* creep model. This subroutine proposed by Hantouche et al. (2018) accounts for the transient creep strains of both A36 and S275 steel material since they have similar yield stress and chemical composition. Then the subroutine is further developed by Al Haddad et al. (2019) to account for the creep of S275 and S355 material by using a modification ratio. Note that, the creep strain rate is represented in the subroutine as a strain-hardening formulation. This formulation results in an accurate prediction of creep strains when the stress history is variable (Hantouche et al., 2018).

B. Thermal Creep Strains of Bolts

When studying the behavior of the flush end-plate connection with the effect of creep in bolts, the subroutine is modified to account for these strains. Matar (2014) proposed a model for the primary creep stage of ASTM A325 bolts based on the steady-

state creep tests. The empirical equation written below predicts with good accuracy the creep bolt strains at temperatures 450, 500, and 550°C (Matar, 2014).

$$\varepsilon_c = \frac{C_1 \sigma^{C_2} t^{C_3+1} e^{-\frac{C_4}{T}}}{C_3 + 1} \quad (2)$$

Where C_1 , C_2 , C_3 , and C_4 are constants specific to each temperature found in Table. 1.

Table.1. Bolt creep constants based on steady-state heating conditions (Matar, 2014).

	450°C	500°C	550°C
C_1	0.000199	3.27×10^{-7}	2.41×10^{-7}
C_2	0.22242	0.854796	0.821356
C_3	-0.92865	-0.77998	-0.51722
C_4	246.5064	2.365149	9.460976

Then these constants are written as a function of temperature to represent transient heating conditions between temperatures 450°C and 600°C. This is based on a linear interpolation of the constants found in Table. 1. Taking into consideration the unit change for the stresses, the constants for transient heating are found in Table. 2.

Table. 2. Bolt creep constants representing transient heating conditions.

	$450^\circ\text{C} \leq T \leq 500^\circ\text{C}$	$500^\circ\text{C} < T \leq 600^\circ\text{C}$
C_1	$(-3.97346 \times 10^{-6}T + 1.987057 \times 10^{-3}) \times 145.038^{C_2}$	$(-1.72 \times 10^{-9}T + 1.187 \times 10^{-6}) \times 145.038^{C_2}$
C_2	$1.264752 \times 10^{-3}T - 5.468964$	$-6.688 \times 10^{-4}T + 1.189196$
C_3	$2.9734 \times 10^{-3}T - 2.26668$	$5.2552 \times 10^{-3}T - 3.40758$
C_4	$-4.882825T + 2443.7776$	$0.14191654T - 68.593121$

To add bolt creep strains to the subroutine, Equation (2) is written as a strain-hardening formulation. Thus, the thermal creep strain difference per iteration is represented as follows:

$$\Delta \varepsilon_c = \left[\left(\frac{C_1 \sigma^{C_2} e^{-\frac{C_4}{T}}}{m} \right)^{\frac{1}{m}} \Delta t (60) + \varepsilon_c^{\frac{1}{m}} \right]^m - \varepsilon_c \quad (3)$$

Where: $m = C_3 + 1$.

As per ABAQUS documentation (Abaqus, 2014), the differentiation of thermal creep strain difference with respect to stress is added to the subroutine and can be written as follows:

$$\frac{d\Delta \varepsilon_c}{d\sigma} = \frac{(0.41368) \Delta t C_2}{\sigma} \left(\frac{C_1 \sigma^{C_2} e^{-\frac{C_4}{T}}}{m} \right)^{\frac{1}{m}} \left[\left(\frac{C_1 \sigma^{C_2} e^{-\frac{C_4}{T}}}{m} \right)^{\frac{1}{m}} \Delta t (60) + \varepsilon_c^{\frac{1}{m}} \right]^{m-1} \quad (4)$$

Adding the creep strains in the analysis is based on an incremental process. At each increment, the stress and temperature are obtained from the ABAQUS simulations and assumed to be constant throughout the increment. Then, the subroutine is used to calculate the creep strains based on the stress, the temperature, and the creep strain history.

CHAPTER III

FE MODEL OF FLUSH END-PLATE CONNECTION

A. Flush End-plate Connection Assemblies

Wang et al. (2011) tested five different connections subjected to transient fire with two degrees of axial restraint at the University of Manchester. Each test was composed of a beam connected by identical connections to two columns as shown in Figure 2. Two of these tests are the flush end-plate connections (Test-3 and Test-8) used in this study. The finite element models of the beam-column flush end-plate connections are developed and validated against the experimental work conducted by (Wang et al., 2011). Note that, ABAQUS implicit solver was used and the post-ultimate response was not considered in the analysis. The FE model predicts the beam axial force, mid-span deflection, and failure mode to be validated with the experimental results. Below are the details of the experiment and the finite element models.

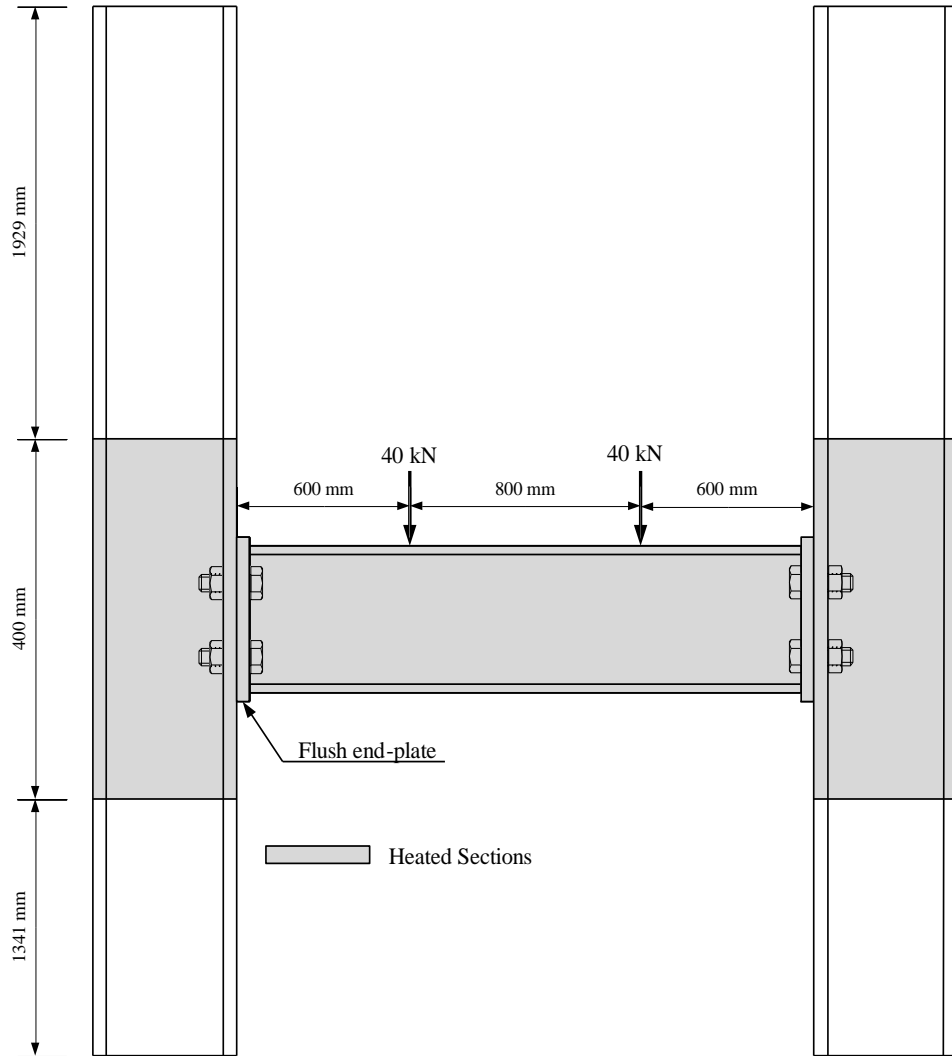


Figure. 2. Flush end-plate connection experimental setup by (Wang et al., 2011).

1. Experimental Data Set

The assemblies were composed of an end-plate welded to the beam and bolted to the column using four M20 bolts. The flush end-plate dimension is 150×200×8 mm, and the beam section is UB 178×102×19 for both assemblies. As labeled by Wang et al. (2011), in Test-3 the column section used is UC 254×254×73, while in Test-8 a smaller column section UC 152×152×23 is used. Both columns have a length of 3.67m and the beam has a length of 2.0m. Detailed dimensions are provided in Figure. 3.

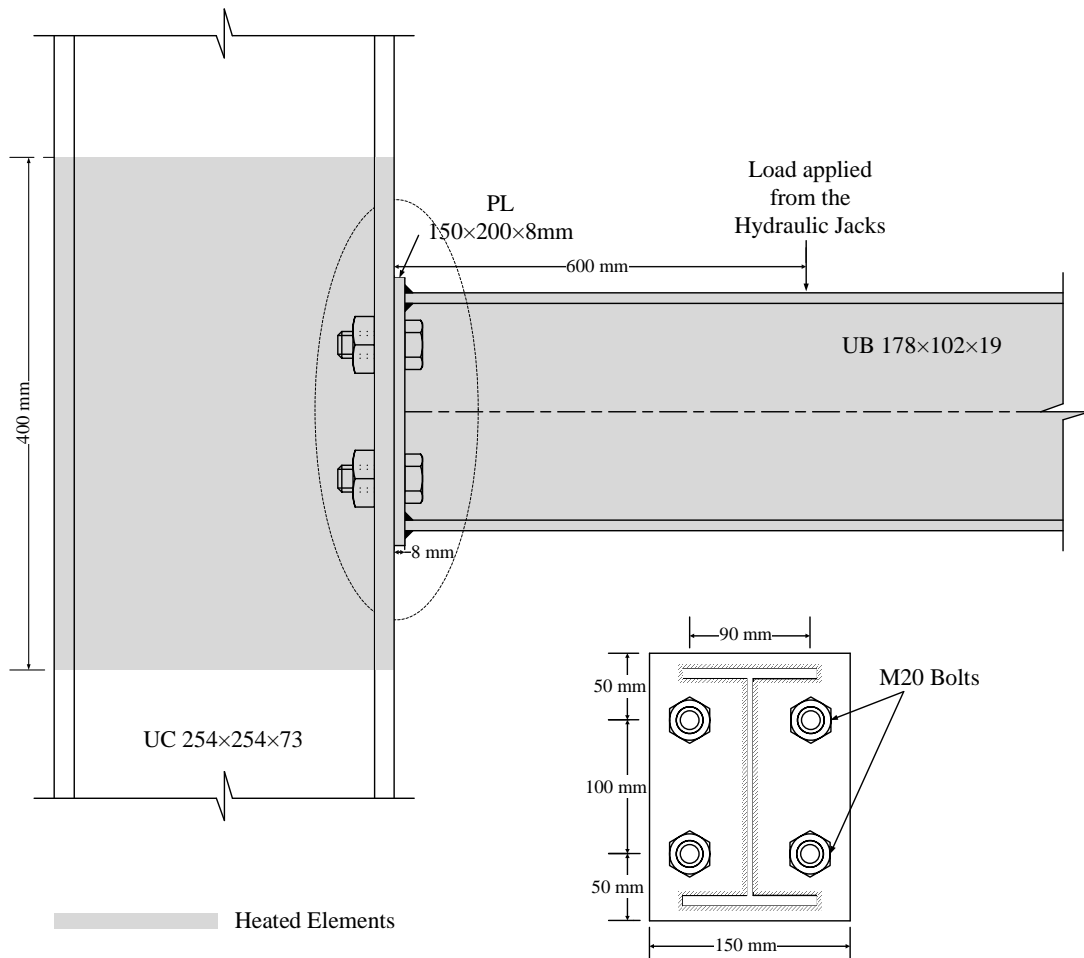


Figure. 3. Dimensions of the proposed flush end-plate connection.

2. Material Properties

An idealized bilinear stress-strain relationship is used for the steel material. The materials used in the FE modeling of the flush end-plate connection are similar to the ones of the experiment. The material for the column section UC 254x254x73 (Test-3) is Grade S355, for the smaller section UC 152x152x23 (Test-8) is Grade S275. Moreover, the beam and end-plate are of grade S275, and the M20 bolts are of Grade 8.8. Tensile coupon tests at ambient conditions taken from the beam sections show that the nominal

strength is 345 Mpa higher than the expected 275 Mpa. *Poisson's* ratio is equal to 0.3 constant at any temperature. The material properties used in the FE models are summarized in Table. 3. To account for the degradation of the material properties at high temperatures, retention factors are used for structural steel and bolt materials proposed by Lee et al. (2013) and Hu et al. (2007), respectively. These factors are based on the creep free stress-strain and temperature relationships for these materials.

Table. 3. Summary of the section and material properties used in FE models.

Section	Column (Test-3) UC 254x254x73	Column (Test-8) UC 152x152x23	Beam UB 178x102x19	End-plate 150x200x300	Bolts M20
E (MPa)	200000	200000	226580	191670	200000
F _y (MPa)	390	344	344	303	800
F _u (MPa)	553	514	514	460	800

B. Description of the FE Model

1. FE Model Discretization

The elements of the flush end-plate connection are meshed using an eight-node brick element with reduced-integration (C3D8-R). The mesh detailing is shown in Figure. 4. The meshing size selected is a 3mm mesh to discretize the bolts and the flush end-plate, 7mm for fine beam mesh, and 15mm for the remaining beam length. The fine mesh is assigned in the area of high stress concentration (around bolt holes and under the concentrated load) and in the area of the connection where members are prone to

failure. A minimum of three mesh elements are used along with the widths of the flush end-plate, beam web and flanges as recommended by Al-Jabri et al. (2006).

Friction is assigned as both tangential and normal behavior with a frictional coefficient of 0.3 and hard contact option, respectively. Contact between surfaces of the model is assigned as finite sliding. This enables the contact surfaces to separate, slide, and rotate.

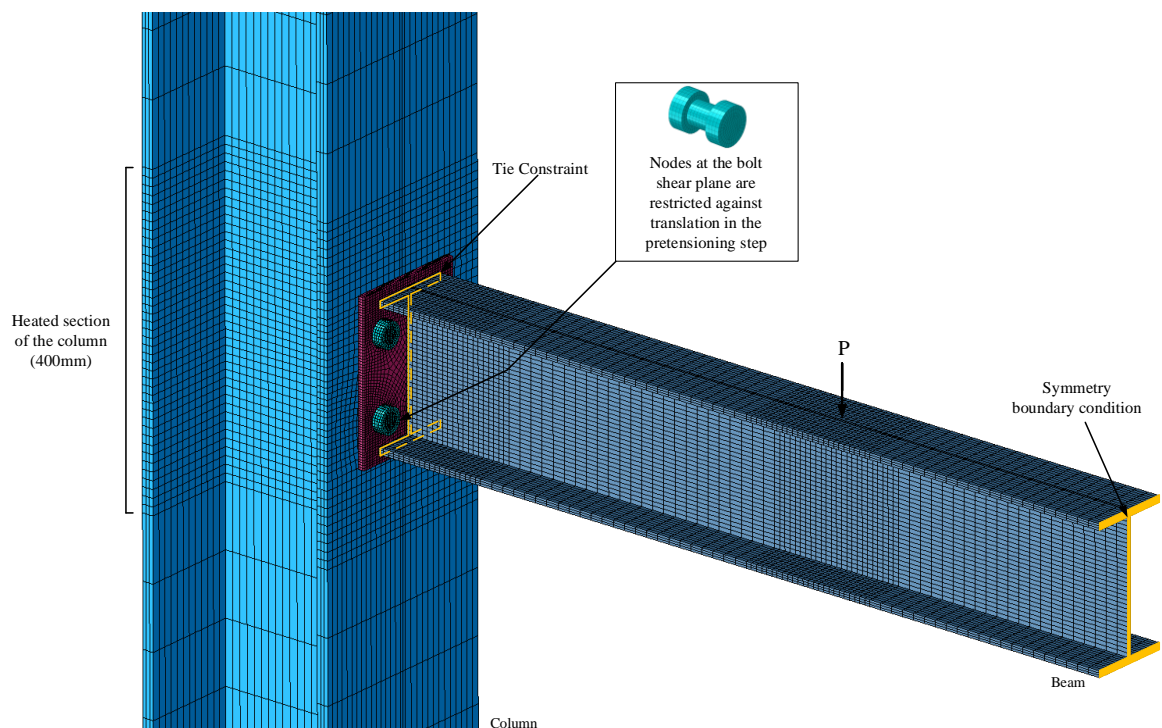


Figure. 4. Flush end-plate connection modeling details.

2. *Boundary Conditions*

The boundary conditions and constraints of the FE model are chosen to represent the framework of the experiment. The test set-up permits the simulation of the column ends as pins while allowing vertical displacement at the top end. Lateral

restraint is assigned to the top beam flange in the model, to represent the effect of a concrete slab. The fillet weld was not modeled, and thus represented as tie constraint between the surfaces of the beam cross-section and the flush end-plate. Due to the symmetry of the geometry and the load, half of the model is simulated. Therefore, a symmetry boundary condition is assigned to the beam's cross-section at mid-span to reduce computational time. The translation of the bolts is restricted only in the pre-tensioning step. Artificial viscous dampers with a damping factor 0.00001 are assigned based on the sensitivity study performed by Dai et al. (2010). These dampers ensure energy dissipation in order to ensure the generation of accurate deformations and to maintain the structural stability of the connection throughout the analysis.

3. Analysis Procedure

The beam-column flush-end plate connection is subjected to fast transient heating conditions following the ISO 834 fire scenario. The connection is loaded as two steps: by applying a direct load on the beam, then heating the connection to the desired temperature while maintaining this load constant. The concentrated load of magnitude 40 kN, corresponding to a load ratio of 50%, is applied using a hydraulic jack at a distance of 0.6 m from the face of the column. In some of the experiments performed by Wang et al. (2011), the hydraulic jacks faced difficulties in maintaining this applied load constant. However, in the FE analysis this concentrated load was constantly applied as pressure on a small area on the beam top flange. The load ratio is defined as a ratio between the simply supported beam's maximum bending moment and the plastic moment strength at ambient temperatures. Then the connection is heated in a furnace of dimensions of 3000×1600×900mm.

The heated elements of the connection are the beam, flush end-plate, bolts, and a 400mm section of the column. Despite the presence of a brick wall in the experiment to uniformly distribute the temperature in the furnace, there was still a maximum of 200°C difference in temperature. Moreover, the beam top flange is covered with a ceramic blanket to represent the effect of the heat-sink of the concrete slab. For the reasons mentioned above, the temperature profile was divided into six regions with different uniform temperature distributions. The temperature profiles used in the validation models of Test-3 and Test-8 are shown in Table. 4.

Table. 4. The temperature profiles of the FE validation models

FE Model	Temperature Profile
Test-3	Beam bottom flange: 730°C
	Beam web: 700°C
	Beam top flange: 450°C
	Connection region: 650°C
	Column heated section: 620°C
	Column unheated section: 20°C
Test-8	Beam bottom flange: 715°C
	Beam web: 700°C
	Beam top flange: 450°C
	Connection region: 650°C
	Column heated section: 620°C
	Column unheated section: 20°C

C. Model Validation

As mentioned above, two experiments were conducted on the flush end-plate connection with different column sizes under transient heating conditions (Wang et al., 2011) The validated models, Test-3 and Test-8, are the connections using the large and small column sections, respectively. Figures. 5. and 6. show that the FE model predicts

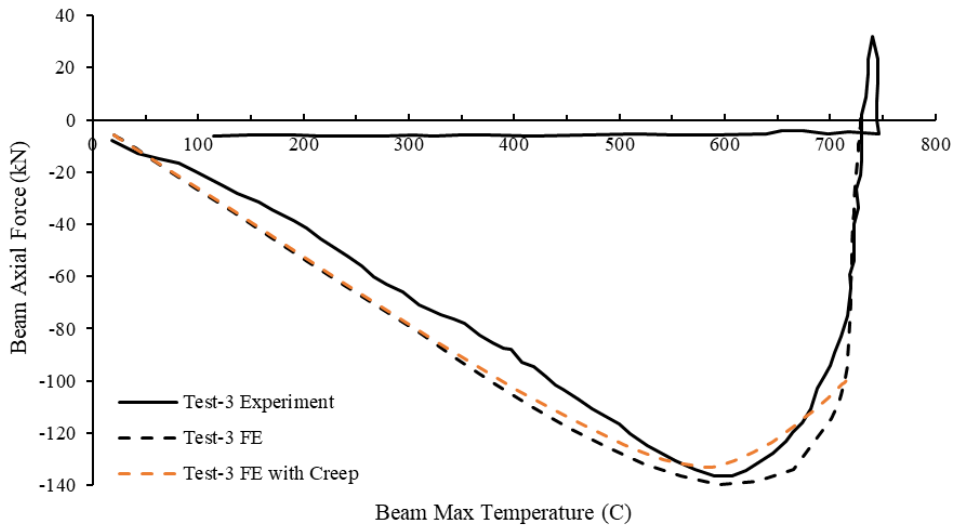
with reasonable accuracy the experimental results as far as beam axial force and mid-span deflection. At low increasing temperatures, the restrained beam undergoes thermal expansion that generates an increase in the compressive beam axial force while maintaining small mid-span deflections. At 600°C (Test-3) and 680°C (Test-8), the beam's compressive axial force starts to decrease indicating the development of the beam catenary action stage. Moreover, at these temperatures, the beam undergoes sagging that generates high mid-span deflections. When comparing the maximum beam axial force of the two connections, it is clear that the larger column section generates larger axial compressive force (139kN vs. 18kN) and similar deflections.

The FE models' failure modes and deformed shapes resemble those of the experiment as shown in Figure. 7. As reported in the experiment of Test-3, the flush end-plate connection failed due to bolt thread stripping and complete detachment. In the experiment of Test-8, the flexibility of the smaller column section reduces the bolt stresses. Thus, preventing the failure of the connection. The failure mode of Test-3 was evident in the FE model by the high stresses generated in the two top bolt shanks. These FE models were capable of predicting the flush end-plate deformation in Test-3 and both the flush end-plate and connected column flange deformations in Test-8.

The thermal creep strains can be ignored in the validation because of the fast heating rate (ISO 834 fire scenario) of the experiment and the non-uniform heating of the components of the flush end-plate connection. However, for the sake of demonstration thermal creep strains are incorporated using Fields and Fields (1988) creep model. Although this model is limited to temperatures below 600°C, the thermal creep strains above this temperature are calculated by considering the material parameters (of Eq. (1)) constant after 600°C. As shown in Fig. 4 and 5, thermal creep

strains have a minimal effect on the validation of the behavior of the flush end-plate connection until this temperature. Thus, in flush end-plate connections under fast transient fires, the effect of thermal creep strains is insignificant and can be ignored.

(a)



(b)

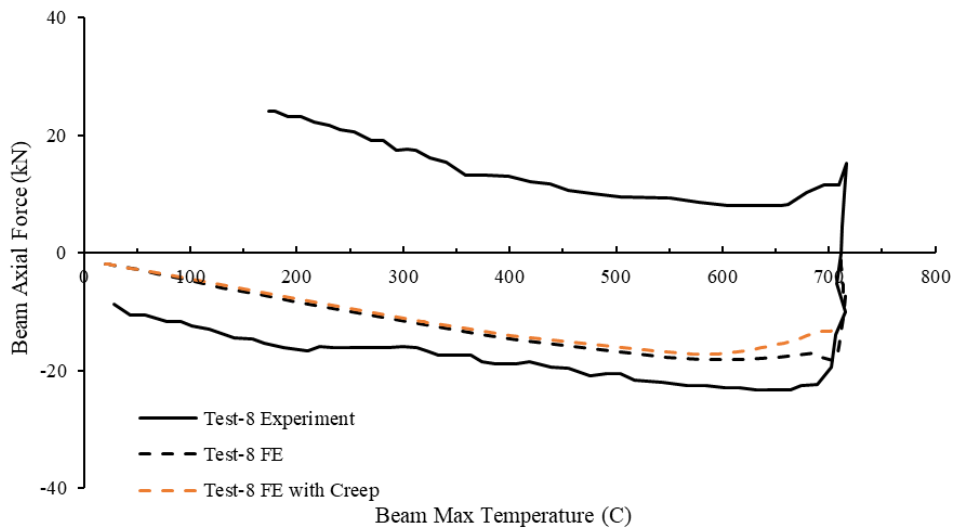
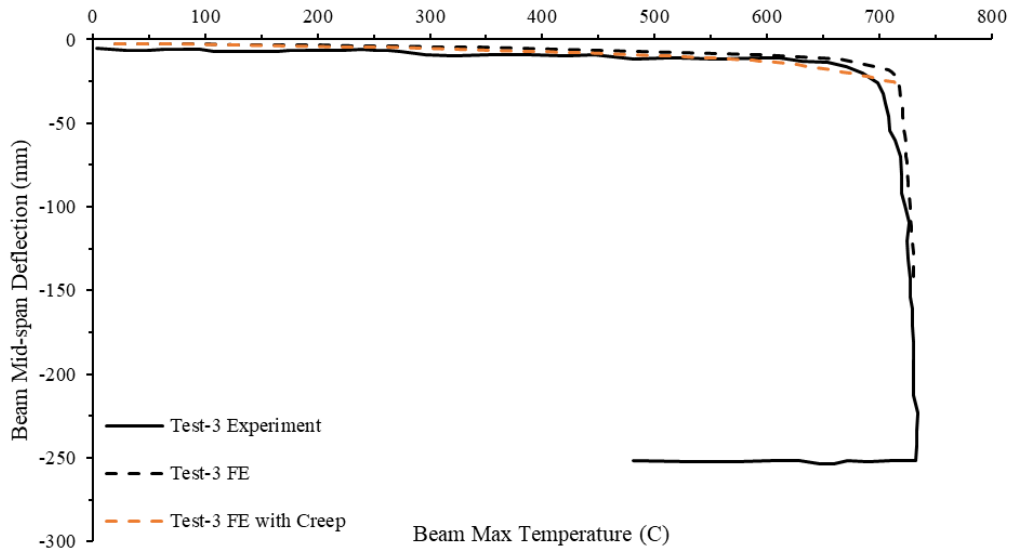


Figure. 5. Comparison between the beam axial force of the experiment and the FE models with and without creep: (a) Test-3; (b) Test-8.

(a)



(b)

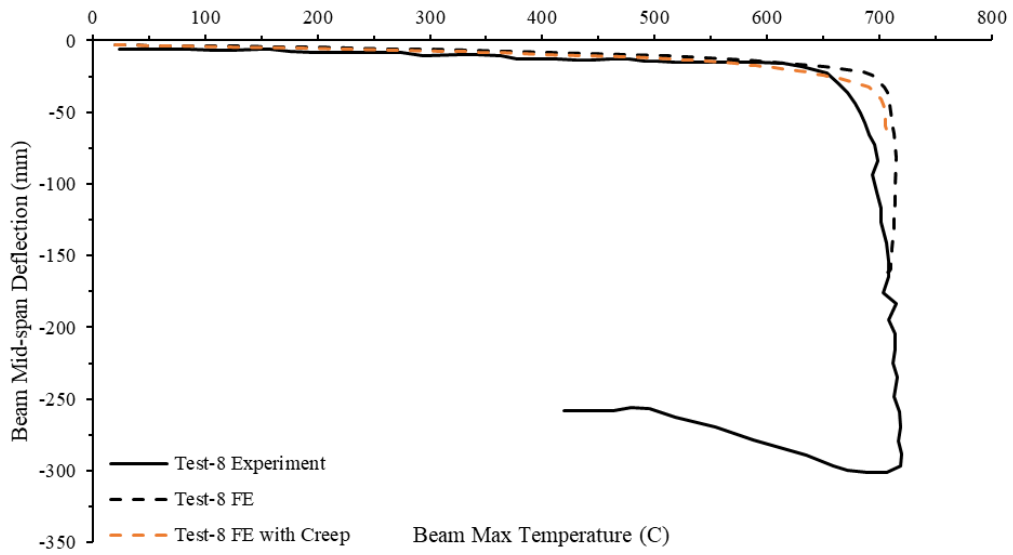
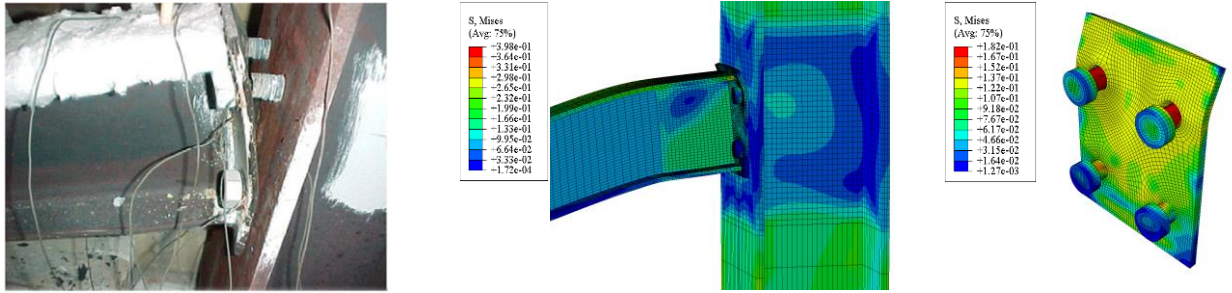


Figure. 6. Comparison between the beam mid-span deflection of the experiment and the FE models with and without creep: (a) Test-3; (b) Test-8.

(a)



(b)

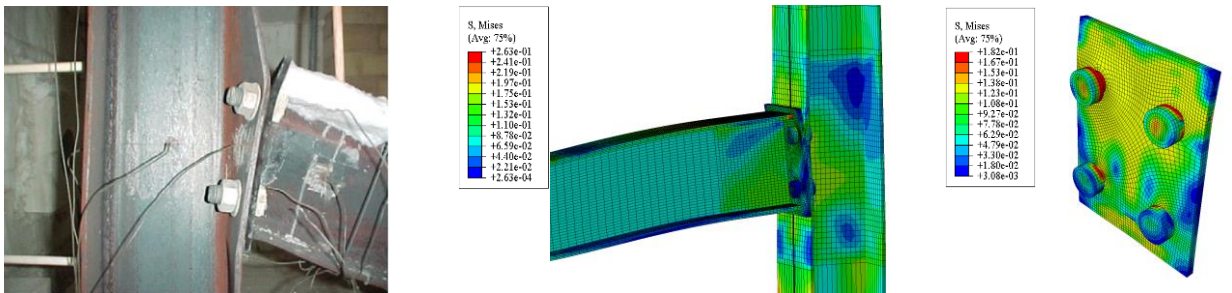


Figure. 7. Comparison between the deformed flush end-plate connection of the experiment (Wang et al., 2011) and the FE models: (a) Test-3; (b) Test-8.

D. Description of the Thermal Creep Model

The thermal creep strains of steel are incorporated in the validated model of Test-3 to study the effect of thermal creep on the behavior of the connection. Thermal creep is explicitly included in the model as a user-defined subroutine and is assigned to the beam, plate and heated part of the column while creep in the bolts is studied later as a parameter. The creep model proposed by Fields and Fields (1988) accounts for thermal creep strains from 350°C to 600°C. Thus, some adjustments are made to the

validated FE model. The maximum heating temperature is uniformly distributed along the heated elements and is limited to 600°C. The heating and cooling phases are based on a linear change between temperatures 20°C and 600°C. When thermal creep strains are included in the analysis, the time of heating and cooling becomes important. The time of exposure to fire depends on the selected heating and cooling rates studied later. In these models, the heating and cooling phases are introduced as ‘VISCO’ steps with tolerance 10^{-5} rather than the ‘General/static’ steps used in the validation models. The ‘VISCO’ step is used when analyzing the time-dependent behavior of steel under transient heating conditions. Note that, there was no need to assign viscous dampers in the models of the parametric studies, for it was numerically stable throughout the analysis. The applied load is equal to 50% of the load ratio, and the heating/cooling rate is 5°C/min unless changed in the parametric studies.

CHAPTER III

PARAMETRIC STUDIES

Extensive parametric studies are performed to understand the behavior of the flush end-plate connection with and without thermal creep. The studied parameters are heating/cooling rate, beam length, load ratio, creep effect in bolts, flush end-plate thickness, and bolt size. The results of these studies are shown below:

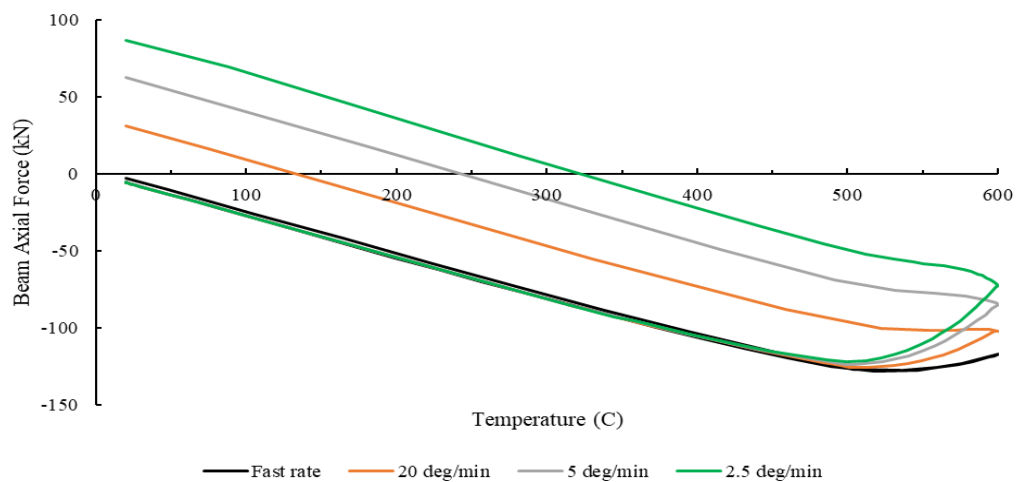
A. Heating/Cooling rate

The change in the temperature of steel depends on the section properties and level of fire protection. For well-insulated sections the rate of change in temperature is 3-7°C/min; however, for poorly-insulated sections, this rate is around 20°C/min (Kodur and Dwaikat, 2010) To study the effect of heating and cooling rate on the flush end-plate connection, different rates are selected 20, 5, and 2.5°C/min. The heating and cooling time for each of the selected rates is 29mins, 116mins, and 232mins, respectively. The results are shown in Figure. 8.

In the fast heating model, the beam thermal expansion causes increased compressive beam axial force while generating small beam mid-span deflections. With the increase of temperatures, the beam loses its load bearing capacity and thus large beam mid-span deflections are observed. When the heating temperature reaches 500°C, the beam enters the catenary action phase. The elements of the connection remain in the elastic region; thus, the strength and stiffness are regained in the cooling phase.

When considering the effect of thermal creep in the models, a reduction in the compressive force accompanied by an increase in the beam mid-span deflection is evident after 500°C. This decrease in the compressive force is due to the stress relaxation of the beam observed in the later stages of fire. When the duration of heating is longer, the stress relaxation increases, thus enhancing the creep effect. The compressive axial force reached at the end of heating is 117, 102, 85, and 73 kN for the fast, 20, 5 and 2.5°C/min, respectively. In the FE models, it is noticeable that the upper part of the end-plate bends more when creep strains are incorporated. This end-plate bending contributes to the increase in the mid-span deflection and the connection rotation. When the structure enters the cooling phase, the axial force continues to decrease, then changes to tension. The slower cooling rates generate higher tensile forces and the beam reaches zero axial force at higher temperatures. For the remaining studied parameters, the heating/cooling rate is taken as 5°C/min.

(a)



(b)

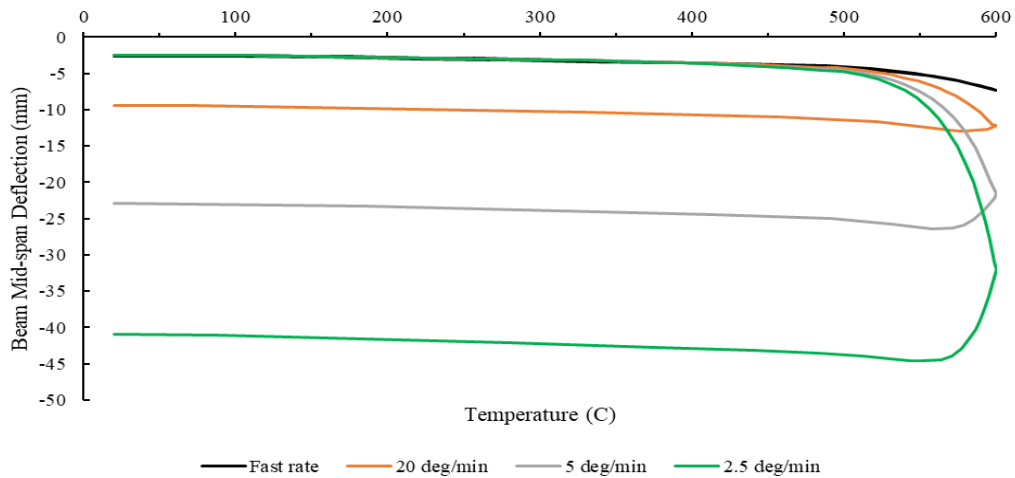


Figure. 8. The effect of different heating and cooling rates on the flush end-plate connection behavior: (a) beam axial force; (b) beam mid-span deflection.

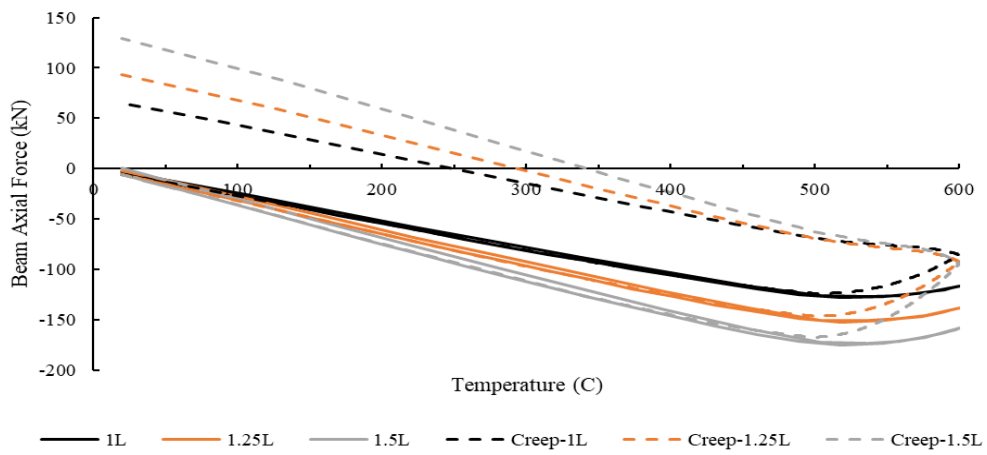
B. Beam Length

The behavior of the flush end-plate connection is investigated using different beam lengths with and without the effect of thermal creep strains. The beam lengths studied are 1L (2 m), 1.25L (2.5 m), and 1.5L (3 m). The applied concentrated loads ensure that the load ratio remains 50% while the beam length is increased.

Figure. 9. shows that the beam with longer span generates larger axial force and mid-span deformation in the fast heating simulations. This is attributed to the fact that as the beam length increases, more surface area is exposed to heating. Thus, larger thermal induced axial forces are generated due to the axial restraint of the column. The beam mid-span deflection is slightly higher throughout the heating and cooling phases when the beam spans are longer.

In thermal creep models, the beam axial compressive force decreases at the end of the heating stage. During the cooling phase, the longer beams generate higher tensile forces. In the creep models, the beam mid-span deflection becomes significantly higher at the end stages of the fire. At the beginning of the cooling phase, this deflection continues to increase then stabilizes and remains constant throughout the cooling phase. At the end of the cooling phase, the mid-span deflection becomes approximately ten times higher than that of the fast heating models.

(a)



(b)

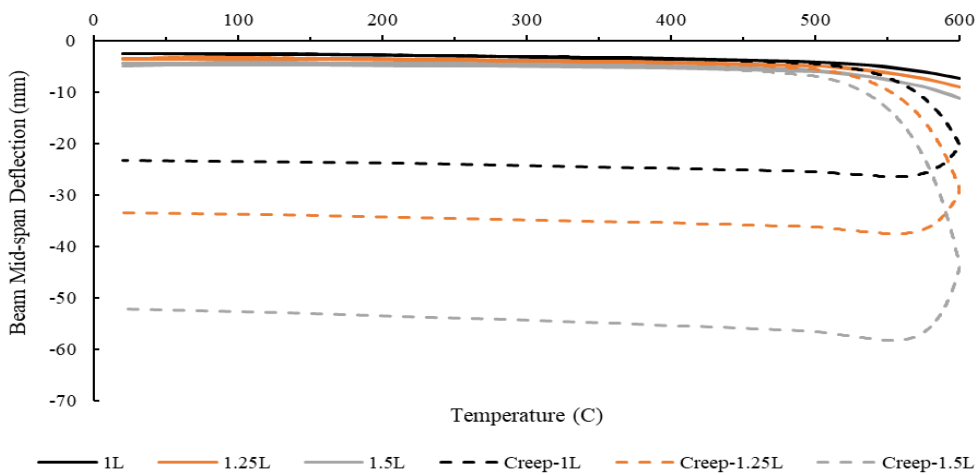


Figure. 9. The effect of beam length on the flush end-plate connection behavior: (a) beam axial force; (b) beam mid-span deflection.

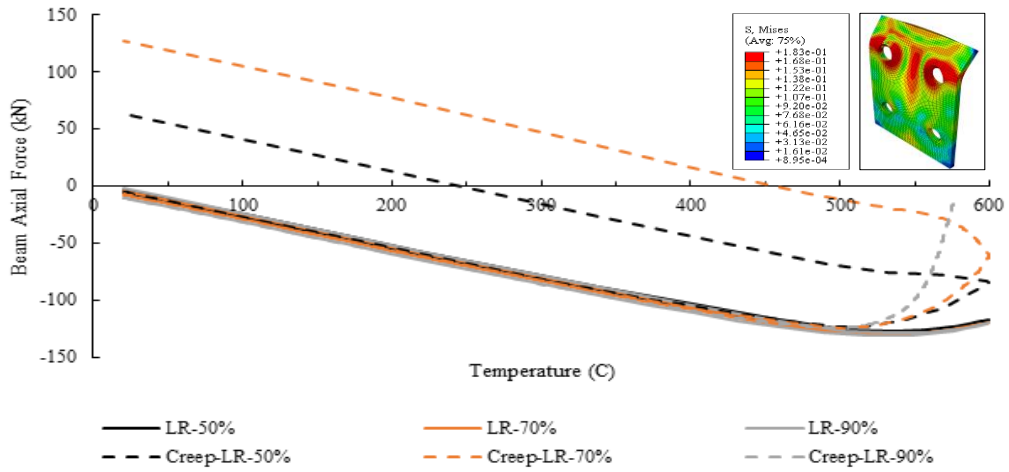
C. Load Ratio

The behavior of the flush end-plate connection when varying the load ratios are shown in Figure. 10. The load ratio is calculated at ambient temperatures as the maximum bending moment of the simply supported beam over its plastic moment capacity. The load ratios are 50%, 70%, and 90% corresponding to concentrated loads of 40 kN, 56 kN, and 72 kN. These loads are calculated based on the nominal strength of the beam tested at ambient (345 Mpa).

The fast heating models show that the applied concentrated load has a negligible effect on the beam axial force during heating or cooling. While the higher applied load generates larger beam mid-span deflection. This shows that the beam axial force under fast heating conditions is mainly generated by the beam thermal expansion. In the fast heating models, some localized partial yielded occurred, in the top beam flange under the location of loading and the connected beam bottom flange.

At a certain load ratio, the effect of thermal creep strains decreases the beam axial force while increasing the beam mid-span deflection towards later stages of fire. As the load ratio increases, the compressive force further decreases during the end of heating while the tensile force increases during the end of the cooling. The mid-span deflection also increases as the load ratio increases. At load ratio of 90%, the creep models generate high stresses in the end-plate along the top bolt row and around the location of the beam web. This indicates a potential fracture in the end-plate or the weld between the beam web and the end-plate.

(a)



(b)

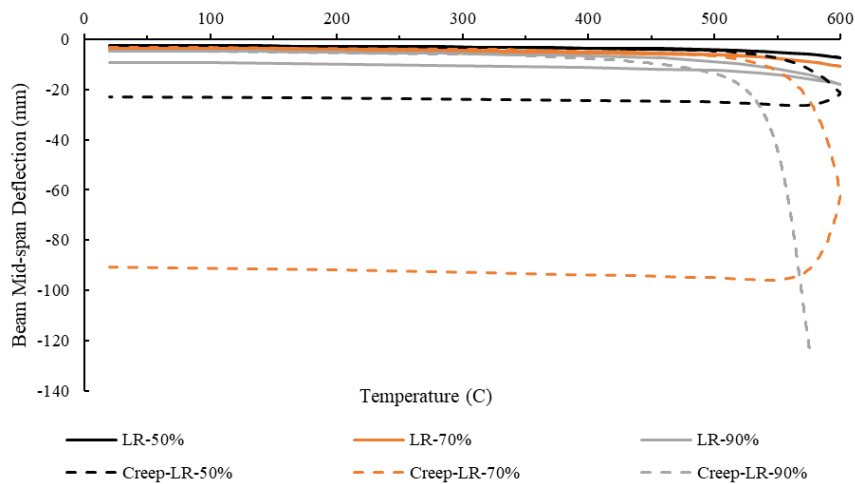


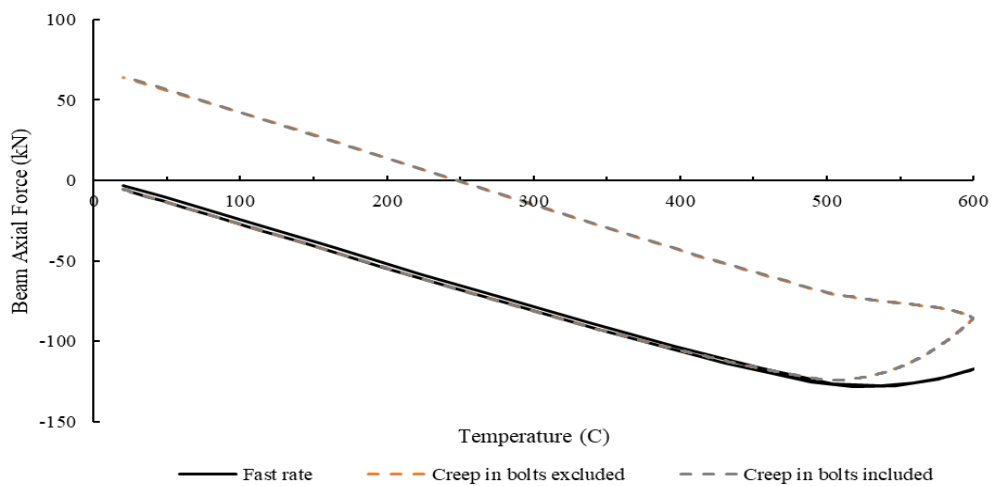
Figure. 10. The effect of load ratio on the flush end-plate connection behavior: (a) beam axial force; (b) beam mid-span deflection.

D. Creep Effect in Bolts

The effect of creep in bolts on the behavior of the flush end-plate connection is plotted in Figure. 11. The thermal creep strains of structural steel were included in the heated part of the column, beam, and flush-end plate based on the equation of Fields and Fields (1988) The thermal creep strains of bolts were assigned to the four bolts of

the connection based on the equation proposed by Matar (2014). The explicit consideration of the thermal creep strains of the structural steel and bolts are incorporated using the subroutine found in the Appendix. When comparing the fast heating models to the thermal creep models of the connection, the compressive axial force of the beam decreased and beam mid-span deflection increased. The creep in bolts has a negligible effect on the global behavior of the connection in terms of the beam axial force and mid-span deflection.

(a)



(b)

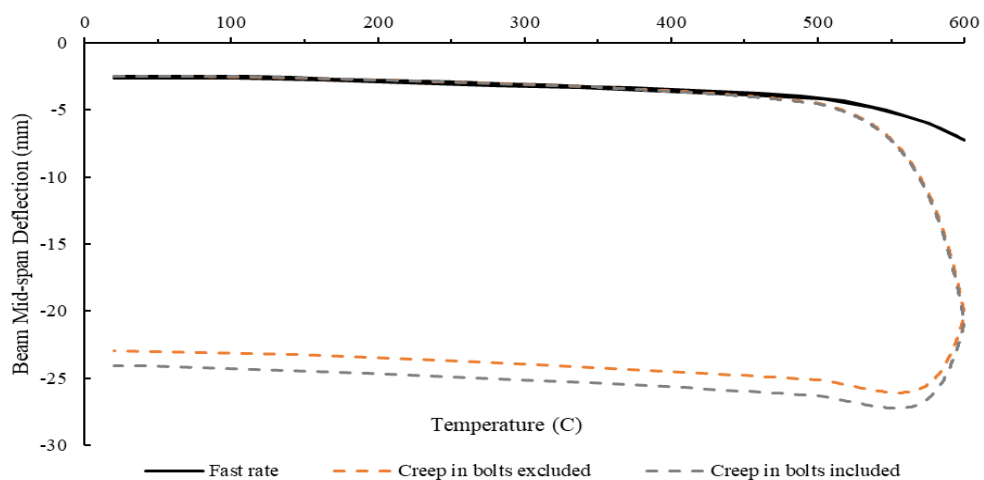
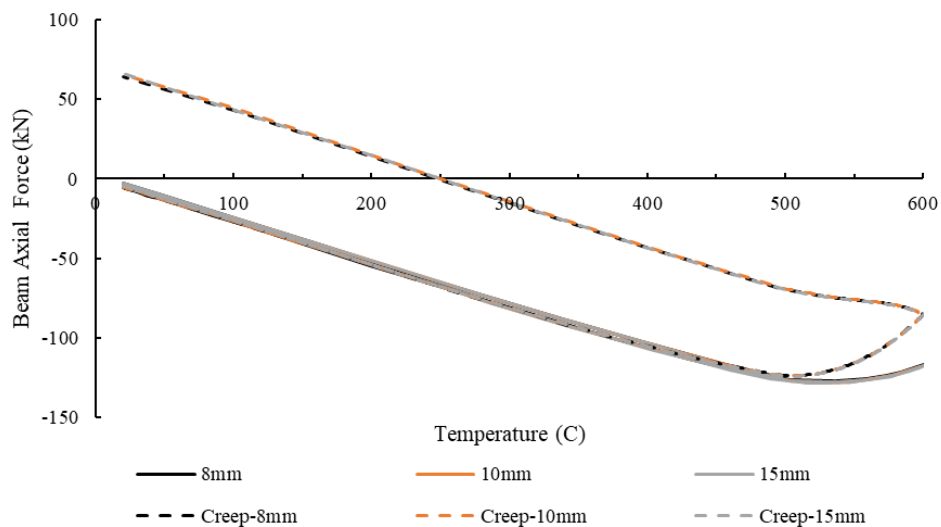


Figure. 11. The effect of creep in bolts on the flush end-plate connection behavior: (a) beam axial force; (b) beam mid-span deflection.

E. Flush End-Plate Thickness and Bolt Size

The plate thicknesses studied are 8, 10, and 15mm and the bolt sizes are M20, M22, and M24. The results are shown in Figures. 12 and 13, respectively. For the fast heating models, these geometrical parameters have no significant effect on beam axial force or mid-span deflection. When including the effect of thermal creep in the analysis, the axial force decreases while the beam mid-span deflection increases during the heating phase. Increasing the flush end-plate thickness and bolt diameter have no impact on the beam axial force. When using a larger bolt diameter, the connection tends to deflect slightly more during the cooling stage. However, increasing the plate thickness reduces the beam mid-span deflection and the bending of the upper part of the end-plate. Thus, giving the connection less rotational ductility.

(a)



(b)

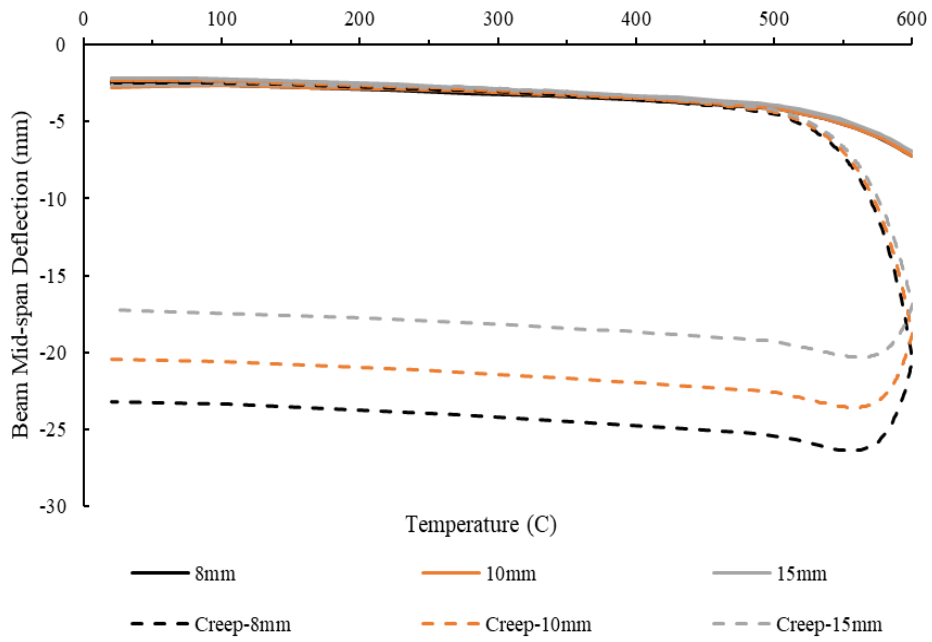
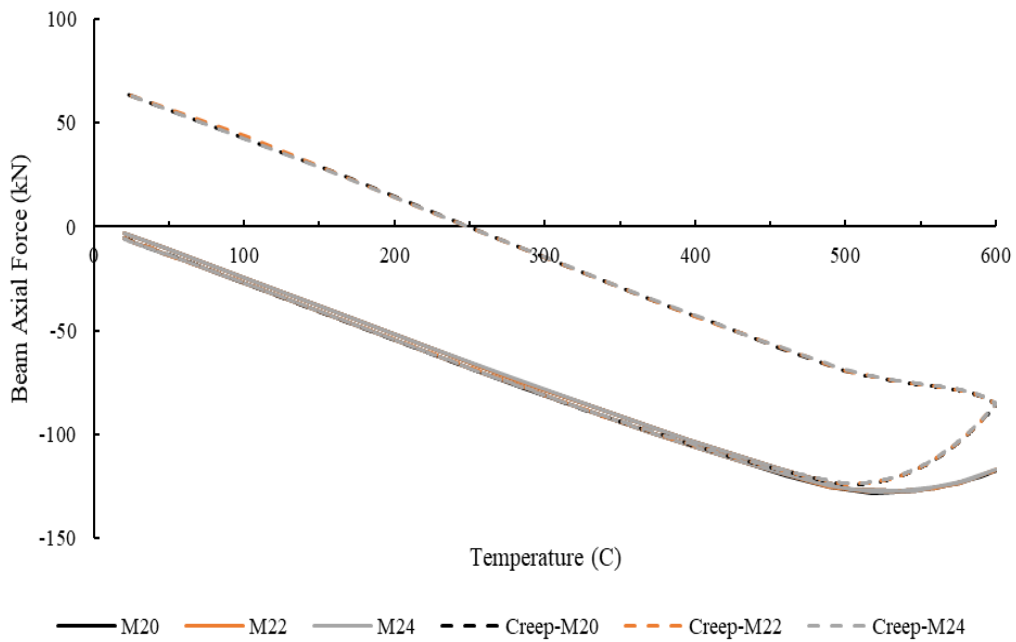


Figure. 12. The effect of plate thickness on the flush end-plate connection behavior: (a) beam axial force; (b) beam mid-span deflection.

(a)



(b)

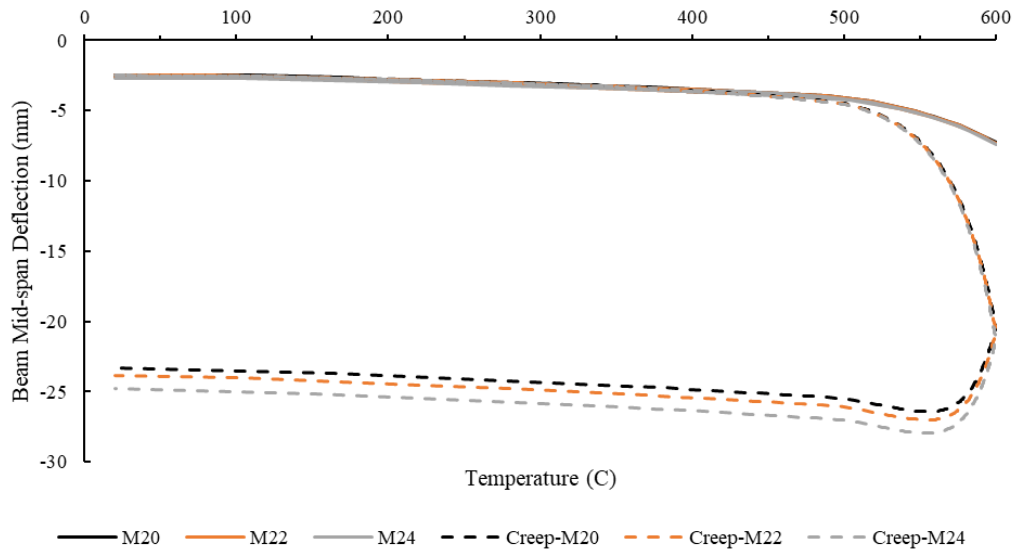


Figure. 13. The effect of bolts size on the flush end-plate connection behavior: (a) beam axial force; (b) beam mid-span deflection.

CHAPTER IV

MECHANICAL MODEL

A mechanical model is proposed to predict the beam axial force of a flush end plate connection in fire while including the effect of thermal creep strains. This proposed model also accounts for the generated high beam mid-span deflections. The development of this model using the component-based approach requires identifying the components of the flush end-plate connection when subjected to high temperatures. These components are described in the model as springs with stiffnesses according to their structural behavior as a part of this connection as shown in Figure. 14.

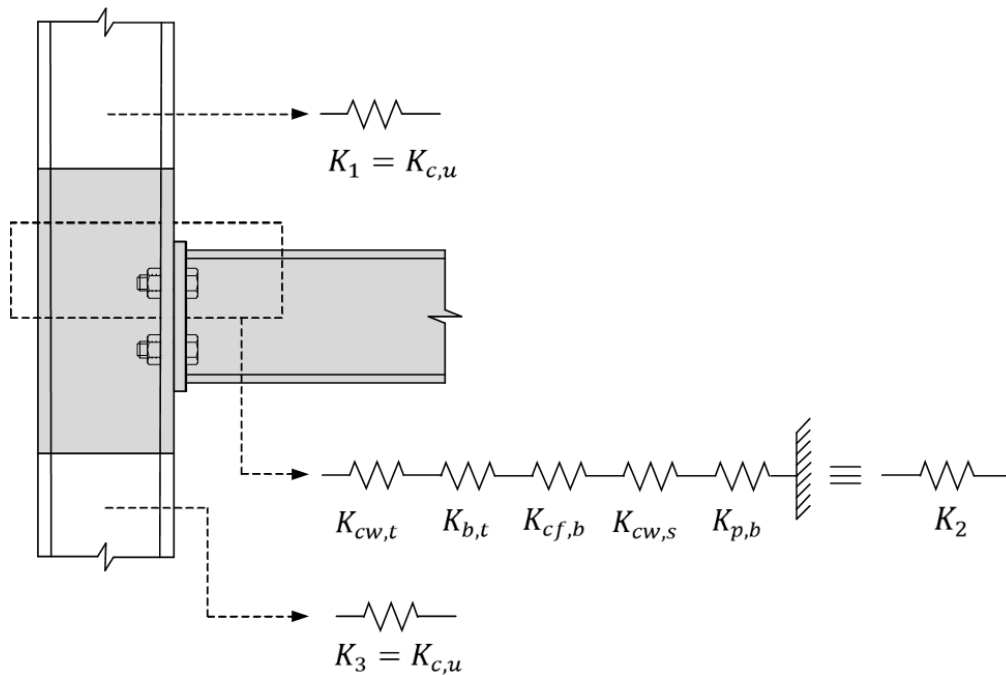


Figure. 14. Components of the flush end-plate connection in fire.

A. Component Stiffness

The mechanical models proposed in the literature are for isolated connections, where the effect of the column length on the stiffness is ignored. Here in this model, the column is studied as three parts: the two unheated sections and the 400 mm heated section. The heated section of the column is divided based on the stiffness of its components, while the unheated sections are considered to have a constant lateral stiffness included in the equivalent connection stiffness. Below are the components of the connection and their corresponding stiffness:

1. Column Web in Tension

The column web acts in tension in the vicinity of the beam flanges and is defined as per Eurocode 3-1.8 (2005) as follows:

$$K_{cw,t} = \frac{0.7b_{eff,cw}t_{cw}}{d_{cw}} E_c \quad (5)$$

where $K_{cw,t}$ is the column web stiffness in tension, $b_{eff,cw}$ is the effective width of the column web calculated as $b_{eff,cw} = 4m + 1.25e$, m is the distance between the fillet and the bolt centerline, e is the distance between the bolt centerline and the edge of the flush-endplate, t_{cw} is the column web thickness, d_{cw} is the effective depth of the column web calculated as $d_{cw} = d_c - 2r_c$, r_c is the fillet angle of the column, E_c is the column elastic modulus.

2. Column Web in Shear

The column web also acts in shear and its stiffness can be written as per Eurocode 3-1.8 (2005):

$$K_{cw,s} = \frac{0.38A_{vc}}{\beta z} E_c \quad (6)$$

where $K_{cw,s}$ is the column web stiffness in shear, A_{vc} is the web shear area of the column and can be calculated as follows $A_{vc} = (h_c - 2t_{cf})t_{cw}$, h_c is the height of the column's cross-section, t_{cf} is the column flange thickness, β is the transformation parameter and taken as 1, z is the lever arm that is the distance between the centerline of the lower column flange and the bolt row in tension.

3. Column Flange in Bending

The column flange acts in bending as per Eurocode 3-1.8 (2005) as follows:

$$K_{cf,b} = \frac{0.9l_{eff,cf}t_{cf}^3}{m^3} E_c \quad (7)$$

where $K_{cf,b}$ is the column flange stiffness in bending, $l_{eff,cf}$ is the effective length of the column flange and is calculated as $l_{eff,cf} = 4m + 1.25e$.

4. Flush End-Plate in Bending

The flush end-plate acts in bending as defined as per Eurocode 3-1.8 (2005) as follows:

$$K_{p,b} = \frac{0.9l_{eff,pb}t_p^3}{m^3} E_p \quad (8)$$

where $K_{p,b}$ is the end-plate stiffness in bending, $l_{eff,pb}$ is the effective length of the end-plate and calculated using the same equation of that of column flange, t_p is the end-plate thickness, E_p is the elastic modulus of the end-plate.

5. Tension Bolts

The stiffness of a tension bolt can be written below:

$$K_{b,t} = \frac{I_{bolt}}{L_{bolt}^3} E_{bolt} \quad (9)$$

where $K_{b,t}$ is the bolt stiffness in tension, n is the number of bolts per row, I_{bolt} is the moment of inertia of the bolts and calculated as follows $I_{bolt} = \frac{\pi d_b^4}{32}$, d_b is the bolt diameter, L_{bolt} is the bolt shank length, E_{bolt} is the elastic modulus of the bolts.

6. Unheated Column

The stiffness of the unheated sections of the column is calculated as follows:

$$K_{c,u} = \frac{12I_c}{L_{c,u}^3} E_{c,u} \quad (10)$$

where $K_{c,u}$ is the stiffness of the unheated column section, I_c is the moment of inertia of the column across its major axis, $L_{c,u}$ is the length of the unheated column section, $E_{c,u}$ is the elastic modulus of the column at ambient.

B. Equivalent Connection Stiffness

The above components of the flush end-plate connection in fire are assembled as an equivalent stiffness K and can be written as:

$$K = \frac{1}{\frac{1}{K} = \frac{1}{K_1} + \frac{1}{K_2} + \frac{1}{K_3}} \quad (11)$$

$$K_1 = K_{c,u} \quad (12)$$

$$K_2 = \frac{1}{\frac{1}{K_{cw,t}} + 2 \times \left(\frac{1}{K_{b,t}} \right) + \frac{1}{K_{cf,b}} + \frac{1}{K_{cw,s}} + \frac{1}{K_{p,b}}} \quad (13)$$

$$K_3 = K_{c,u} \quad (14)$$

C. Beam Axial Force

This proposed model predicts the thermal beam axial force acting on the flush end-plate connection at elevated temperatures including the effect of thermal creep strains. This model is able to predict the compressive force during the heating stage and the tensile forces during the cooling stage.

1. Fast Analysis

After calculating the equivalent stiffness of the flush end-plate connection, a simple representation consisting of the connection equivalent stiffness and the beam axial stiffness can be established. In the fast analysis, the beam axial force can be written as proposed by El Kalash and Hantouche (2017) :

$$\Delta P_i = \frac{KE_b A_b \alpha (\Delta T)}{\left(\frac{E_b A_b}{L_b} \right) + K} \quad (15)$$

where ΔP_i is the incremental beam axial force, E_b is the beam elastic modulus, A_b is the beam cross-sectional area contributing to the beam axial force, α is the coefficient of thermal expansion, ΔT is the incremental change in temperature and depends on the heating/cooling rate, L_b is the beam length. Knowing that the FE model follows a transient heating condition, the compressive axial force at each increment (P_i) is the summation of the generated axial force of this increment (ΔP_i) and the previous one ($P_{(i-1)}$).

$$P_i = \Delta P_i + P_{(i-1)} \quad (16)$$

In the heating stage, the beam expands and develops a compressive axial force in the early stages of fire. However, at temperatures above 500°C, the beam axial force

decreases changing from compression into tension and initiating the catenary action phase.

The effect of the beam mid-span deflection is significant to consider on the beam axial force, especially when thermal creep of steel is considered. Thus, the $P - \Delta$ effect will be added by considering these stresses over the cross-sectional area that contributes to the beam axial force. Then the beam axial force is calculated using the following equation:

$$\Delta P_i = \frac{KE_b A_b \alpha (\Delta T)}{\left(\frac{E_b A_b}{L_b}\right) + K} + \left(\frac{P_{(i-1)} \delta}{I_b}\right) y A_b \quad (17)$$

where δ is the beam mid-span deflection relative to each temperature, and I_b is the moment of inertia of the beam, and y is equal to half of the beam depth.

The FE beam mid-span deflection result (δ) of each parameter is curve fitted into equations written as a function of temperatures found in Table 5 (found in subsection 'E' of this chapter). In the fast analysis, the beam strength and stiffness are restored; thus, the same deflection equations found in Table 5 can be used for the heating and cooling phases.

2. Thermal Creep Analysis

The effect of thermal creep depends on three factors: stress, time, and temperature. At each increment, all these factors are considered constants. The value of the time increment is considered to be 1 minute, while the value of the temperature increment depends on the heating and the cooling rate.

Before 350°C, the effect of creep is insignificant at low temperatures; thus, the same procedure is used as that of the fast analysis. At temperatures between 350°C and

600°C, this mechanical model incorporates the Fields and Fields (1988) creep model directly and estimates the thermal creep strains. The equation of this model, along with the unit conversions and constants, is written below:

$$\varepsilon_c = 0.01at^b \left(145.038\sigma_{fast}\right)^c \quad (18)$$

$$T < 350^\circ C \quad a = 0 \quad (19)$$

$$350^\circ C \leq T < 500^\circ C \quad a = 10^{-(6.1+0.00573T)} \quad (20)$$

$$500^\circ C \leq T < 600^\circ C \quad a = 10^{-(13.25-0.00851T)} \quad (21)$$

$$b = -1.1 + 0.0035T \quad (22)$$

$$c = 2.1 + 0.0064T \quad (23)$$

The stress is required to be substituted in Eqn. (18) to compute the corresponding creep strains at a specific time and temperature. This stress can be calculated as an approximation from the fast analysis as beam axial force distributed over the effective cross-sectional area at a specific time and temperature. The beam is considered elastic in the fast analysis at the mid-span cross-sectional area, and thus the stress can be calculated as:

$$\sigma_{fast} = \frac{P_{fast}}{A} \quad (24)$$

After creep strains are obtained, the creep stress can be calculated below using the equation below:

$$\sigma_c = E_b \times \varepsilon_c \quad (25)$$

Then the beam axial force with the inclusion of thermal creep strains is calculated by adding the beam axial force under fast heating conditions to the stresses due to $P - \Delta_c$ and thermal creep effect multiplied by the effective beam cross-sectional area.

$$P_c = P_{fast} + (\sigma_M + \sigma_c)A_b \quad (26)$$

The stress (σ_M) due to $P - \Delta_c$ is calculated using the beam mid-span deflection when creep is incorporated (δ_c). The equations of the mid-span deflection in the heating and cooling phases are found in Table 6 (found in subsection ‘E’ of this chapter).

$$\sigma_M = \left(\frac{P_{(i-1)} \delta_c}{I_b} \right) y A_b \quad (27)$$

In the cooling phase, the creep strains are estimated to be composed of the creep strains at 600°C magnified by a constant (N) and the creep strain at each cooling temperature calculated using Eqn. 16. Thus the creep cooling stresses are calculated as follows:

$$(\sigma_c)_{cooling} = N(\sigma_c)_{600^\circ C} + (\sigma_c)_T \quad (28)$$

where $T < 600^\circ C$ and (N) is a constant that depends on the parameters that increase the effect of creep strains on the flush end-plate connection. This constant, in the form of an equation, is written below:

$$N = \frac{R^{0.22} LR^3}{0.5^3 L_b} \quad (29)$$

where R is the heating/cooling rate substituted by 2.5, 5, and 20 for heating/cooling rates 2.5, 5, and 20°C/min. LR is the load ratio substituted by 0.5, 0.7, and 0.9 for load ratios 50%, 70%, and 90%. L_b is the beam length substituted by 1, 1.25, and 1.5 for beam lengths 1L, 1.25L, and 1.5L.

D. Flush End-plate Connection Limit State

The limit state of the flush end-plate connection in fire is the end-plate flexural yielding as shown in the results of the FE analysis. This was shown in the load ratio parameter,

where the connection was subjected to two concentrated loads equivalent to a 90% load ratio with the consideration of thermal creep. The end-plate has yielded when the moment applied on the connection is equal to the moment nominal capacity of the end-plate in bending (M_n) according to the yield-line mechanism. The capacity is calculated based on the AISC steel design guide (Murray and Shoemaker, 2002) written below:

$$M_n = f_{py} t_p^2 Y \quad (30)$$

where f_{py} is the yield strength of the end-plate material and Y is calculated as follows:

$$Y = \frac{h_1 b_p}{2} \left(\frac{1}{p_f} + \frac{1}{s} \right) + \frac{2h_1}{g} (p_f + s) \quad (31)$$

where is the h_1 distance from the lower beam flange to the center of the first bolt row, b_p is the width of the end-plate, g is the center to center distance between the bolts in a bolt row, p_f is the distance between the center of the first bolt row and the lower end of the beam top flange, s is calculated as the follows:

$$s = 0.5 \sqrt{b_p g} \quad (32)$$

Note that, use $p_f = s$, if $p_f > s$

E. Beam Mid-span Deflection

The beam mid-span deflections used for the prediction of the beam thermal induced forces are obtained from the FE analysis. In the tables below, the beam mid-span deflections are written as equations in terms of temperature for fast and prolonged heating conditions.

Table 5. Beam mid-span deflection of all parameters subjected to fast heating.

Length= 1L Load Ratio 50%	$T \leq 350^{\circ}C$	$\delta = -(5.97 \times 10^{-6})T^2 - (2.92 \times 10^{-4})T - 2.44$
	$350^{\circ}C < T \leq 500^{\circ}C$	$\delta = -(1.5 \times 10^{-5})T^2 + (7.47 \times 10^{-3})T - 4.05$
	$500^{\circ}C < T \leq 600^{\circ}C$	$\delta = -(9.75 \times 10^{-7})T^3 + (1.37 \times 10^{-3})T^2 + (6.52 \times 10^{-1})T - 101$
Parameter beam length Length= 1.25L	$T \leq 350^{\circ}C$	$\delta = -(7.58 \times 10^{-6})T^2 + (9.52 \times 10^{-4})T - 3.38$
	$350^{\circ}C < T \leq 500^{\circ}C$	$\delta = -(2.24 \times 10^{-5})T^2 + (1.34 \times 10^{-2})T - 5.91$
	$500^{\circ}C < T \leq 600^{\circ}C$	$\delta = -(1.419 \times 10^{-6})T^3 + (2.013 \times 10^{-3})T^2 - (9.657 \times 10^{-1})T + 152$
Parameter beam length Length= 1.5L	$T \leq 350^{\circ}C$	$\delta = -(9.45 \times 10^{-6})T^2 + (2.54 \times 10^{-4})T - 4.46$
	$350^{\circ}C < T \leq 500^{\circ}C$	$\delta = -(3.47 \times 10^{-5})T^2 + (2.3 \times 10^{-2})T - 8.52$
	$500^{\circ}C < T \leq 600^{\circ}C$	$\delta = -(2.041 \times 10^{-6})T^3 + (2.932 \times 10^{-3})T^2 - 1.423T + 227.6$
Parameter load ratio Load ratio 70%	$T \leq 350^{\circ}C$	$\delta = -(8.99 \times 10^{-6})T^2 + (2.59 \times 10^{-4})T - 3.47$
	$350^{\circ}C < T \leq 500^{\circ}C$	$\delta = -(2.47 \times 10^{-5})T^2 + (1.28 \times 10^{-2})T - 6.11$
	$500^{\circ}C < T \leq 600^{\circ}C$	$\delta = -(1.531 \times 10^{-6})T^3 + (2.162 \times 10^{-3})T^2 - 1.034T + 161.8$
Parameter load ratio Load ratio 90%	$T \leq 350^{\circ}C$	$\delta = -(1.25 \times 10^{-5})T^2 - (1.6 \times 10^{-4})T - 4.57$
	$350^{\circ}C < T \leq 500^{\circ}C$	$\delta = -(1.15 \times 10^{-4})T^2 + (8.02 \times 10^{-2})T - 20.2$
	$500^{\circ}C < T \leq 600^{\circ}C$	$\delta = -(7.504 \times 10^{-4})T^2 + (7.384 \times 10^{-1})T - 190.7$

Table 6. Beam mid-span deflection of all parameters subjected to heating while considering the effect of thermal creep; (a) heating phase, (b) cooling phase.

(a)

Parameter heating/cooling rate Rate= 2.5°C/min	$T \leq 350^{\circ}C$	$\delta_c = -(6.87 \times 10^{-6})T^2 + (6.5 \times 10^{-5})T - 2.45$
	$350^{\circ}C < T \leq 500^{\circ}C$	$\delta_c = -(4.39 \times 10^{-5})T^2 + (2.78 \times 10^{-2})T - 7.66$
	$500^{\circ}C < T \leq 600^{\circ}C$	$\delta_c = -(5.032 \times 10^{-5})T^3 + (7.916 \times 10^{-2})T^2 - 41.56T - 7276$
Parameter heating/cooling rate Rate= 5°C/min	$T \leq 350^{\circ}C$	$\delta_c = -(7.31 \times 10^{-6})T^2 + (1.71 \times 10^{-4})T - 2.46$
	$350^{\circ}C < T \leq 500^{\circ}C$	$\delta_c = -(3.12 \times 10^{-5})T^2 + (1.83 \times 10^{-2})T - 5.9$
	$500^{\circ}C < T \leq 600^{\circ}C$	$\delta_c = -(2.44 \times 10^{-5})T^3 + (3.082 \times 10^{-2})T^2 - 19.79T - 3436.2$

Parameter heating/cooling rate Rate= 20°C/min	$T \leq 350^\circ C$	$\delta_c = -(6.63 \times 10^{-6})T^2 - (2.92 \times 10^{-5})T - 2.45$
	$350^\circ C < T \leq 500^\circ C$	$\delta_c = -(1.36 \times 10^{-5})T^2 + (4.86 \times 10^{-3})T - 3.31$
	$500^\circ C < T \leq 600^\circ C$	$\delta_c = -(7.644 \times 10^{-6})T^3 + (1.174 \times 10^{-2})T^2 - 6.039T - 1036$
Parameter beam length Length= 1.25L	$T \leq 350^\circ C$	$\delta_c = -(6.41 \times 10^{-6})T^2 - (6.04 \times 10^{-4})T - 3.39$
	$350^\circ C < T \leq 500^\circ C$	$\delta_c = -(4.03 \times 10^{-5})T^2 + (2.44 \times 10^{-2})T - 7.63$
	$500^\circ C < T \leq 600^\circ C$	$\delta_c = -(3.426 \times 10^{-5})T^3 + (5.356 \times 10^{-2})T^2 - 27.98T - 4877$
Parameter beam length Length= 1.5L	$T \leq 350^\circ C$	$\delta_c = -(1.06 \times 10^{-5})T^2 - (3.08 \times 10^{-3})T - 4.49$
	$350^\circ C < T \leq 500^\circ C$	$\delta_c = -(6.95 \times 10^{-5})T^2 + (4.55 \times 10^{-2})T - 12.2$
	$500^\circ C < T \leq 600^\circ C$	$\delta_c = -(5.492 \times 10^{-5})T^3 + (8.595 \times 10^{-2})T^2 - 44.94T - 7842$
Parameter load ratio Load ratio 70%	$T \leq 350^\circ C$	$\delta_c = -(9.29 \times 10^{-6})T^2 + (1.39 \times 10^{-4})T - 3.14$
	$350^\circ C < T \leq 500^\circ C$	$\delta_c = -(5.89 \times 10^{-5})T^2 + (3.53 \times 10^{-2})T - 9.45$
	$500^\circ C < T \leq 600^\circ C$	$\delta_c = -(1.3614 \times 10^{-1})T^3 + (2.1631 \times 10^{-1})T^2 - 114.61T + 20239$
Parameter load ratio Load ratio 90%	$T \leq 350^\circ C$	$\delta_c = -(1.28 \times 10^{-5})T^2 - (1.37 \times 10^{-4})T - 4.58$
	$350^\circ C < T \leq 500^\circ C$	$\delta_c = -(2.59 \times 10^{-4})T^2 + (1.76 \times 10^{-1})T - 36.5$
	$500^\circ C < T \leq 600^\circ C$	$\delta_c = -(3.4941 \times 10^{-1})T^3 + (5.3365 \times 10^{-1})T^2 - 271.82T + 46159$

(b)

Parameter heating/cooling rate Rate= 2.5°C/min	$600^\circ C > T \geq 500^\circ C$	$\delta_c = (5.8933 \times 10^{-5})T^3 - (9.4561 \times 10^{-2})T^2 + 50.504T - 9022.51$
	$T < 500^\circ C$	$\delta_c = -(5.597 \times 10^{-6})T^2 - (2.856 \times 10^{-3})T - 40.87$
Parameter heating/cooling rate Rate= 5°C/min	$600^\circ C > T \geq 500^\circ C$	$\delta_c = (2.7791 \times 10^{-5})T^3 - (4.4673 \times 10^{-2})T^2 + 23.884T - 4272.9$
	$T < 500^\circ C$	$\delta_c = -(5.472 \times 10^{-6})T^2 - (1.826 \times 10^{-3})T - 22.79$
Parameter heating/cooling rate Rate= 20°C/min	$600^\circ C > T \geq 500^\circ C$	$\delta_c = (8.5582 \times 10^{-6})T^3 - (1.3918 \times 10^{-2})T^2 + 7.5134T - 1358.3$
	$T < 500^\circ C$	$\delta_c = -(6.877 \times 10^{-6})T^2 - (4.514 \times 10^{-4})T - 9.4$
Parameter beam length Length= 1.25L	$600^\circ C > T \geq 500^\circ C$	$\delta_c = (4.3629 \times 10^{-5})T^3 - (7.0202 \times 10^{-2})T^2 + 3.7596T - 6738.2$
	$T < 500^\circ C$	$\delta_c = -(5.611 \times 10^{-6})T^2 - (2.894 \times 10^{-3})T - 33.36$
Parameter beam length Length= 1.5L	$600^\circ C > T \geq 500^\circ C$	$\delta_c = (7.2737 \times 10^{-5})T^3 - (1.1711 \times 10^{-1})T^2 + 62.764T - 11255$
	$T < 500^\circ C$	$\delta_c = -(6.208 \times 10^{-6})T^2 - (5.762 \times 10^{-3})T - 52.07$
Parameter load ratio Load ratio 70%	$600^\circ C > T \geq 500^\circ C$	$\delta_c = (1.6376 \times 10^{-4})T^3 - (2.636 \times 10^{-1})T^2 + 141.28T - 25307$
	$T < 500^\circ C$	$\delta_c = -(7.396 \times 10^{-6})T^2 - (5.291 \times 10^{-3})T - 90.5$

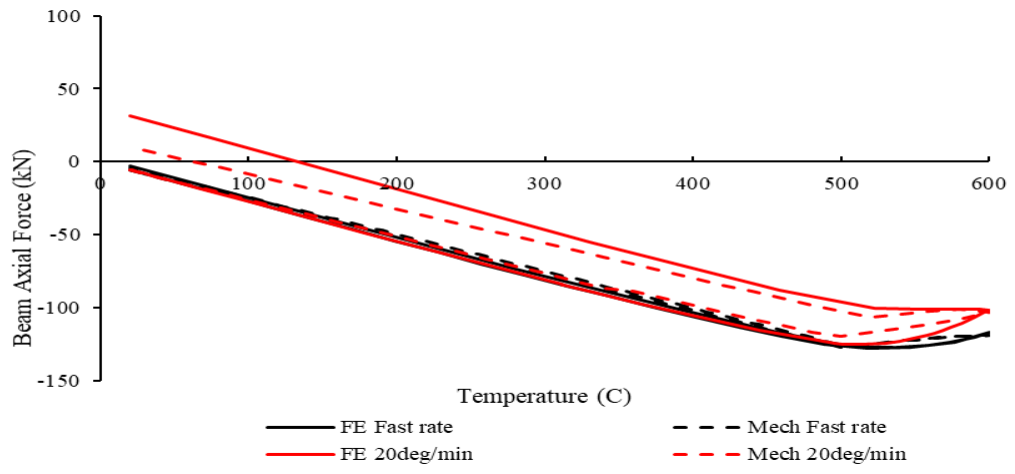
F. Model Performance

The mechanical model performance is compared with the results of the finite element simulations. This comparison is performed on the studied parameters with and without the inclusion of thermal creep strains. The FE parametric studies showed that the parameters to be considered are the heating/cooling rate, beam length, and the load ratio. While the remaining parameters, such as the creep effect in bolts, flush end-plate thickness, and the bolt diameter had a negligible effect on the response of the flush end-plate connection.

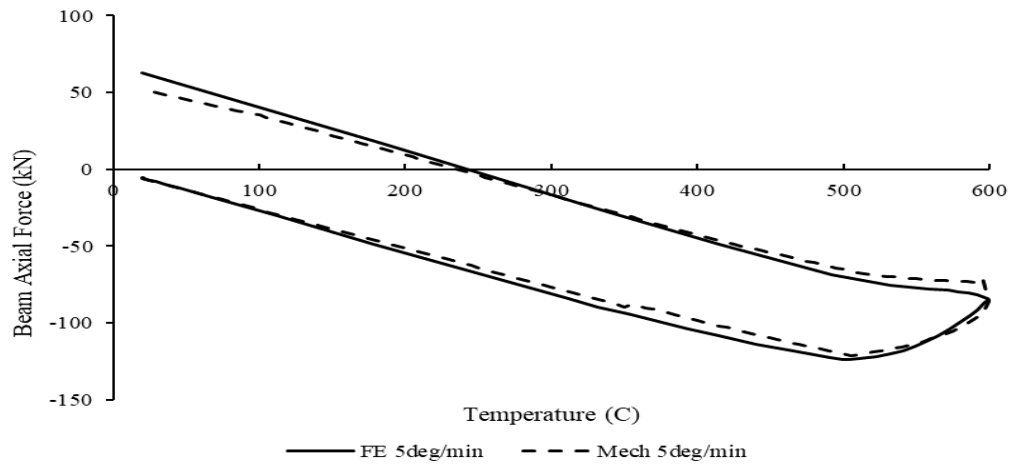
The results of the major parameter are shown separately in Figures 15, 16, and 17. It can be seen that the mechanical model predicts with acceptable accuracy the beam axial force of the flush end-plate connection in the heating and cooling phases under transient heating conditions.

In Figure. 15, the results of changing the heating rate are presented. In the fast heating rate and at temperatures higher than 500°C, the beam enters the catenary action phase and the compressive beam axial force starts to decrease. To account for different heating/cooling rates in the mechanical model, each increment has a specific (ΔT) based on the rate while the time increment is considered as 1 minute. Thus, (ΔT) is substituted as 20, 5, and 2.5 for the rates 20, 5, and 2.5deg/min. As shown below, the proposed model can predict the thermal creep effect on the beam axial force when subjected to different heating/cooling rates. As the rate decreases, the effect of creep is amplified where the reduction of compressive forces is higher at the end of the heating phase. Moreover, the generated tensile forces are larger at the end of the cooling phase.

(a)



(b)



(c)

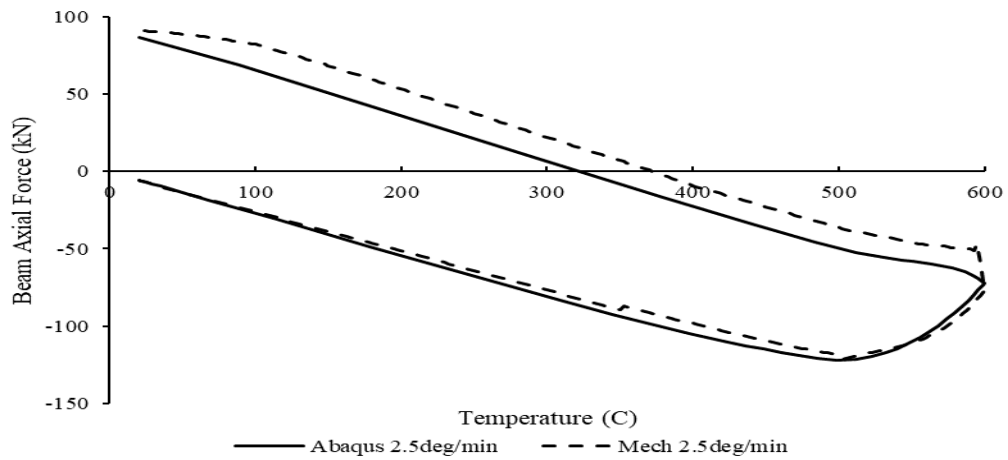


Figure. 15. Mechanical model results on the heating/cooling rate parameter with and without creep; (a) Fast rate and 20deg/min; (b) 5deg/min; (c) 2.5deg/min.

The results of the mechanical model when varying the beam length of the flush end-plate connection are found in Figure.16. The mechanical model predicts the beam axial force with reasonable accuracy in the fast and prolonged heating conditions. In the fast heating models, the beam axial force was larger due to the longer heated beam spans. When the creep strains are incorporated, the mechanical model captured the decrease in the beam axial compressive at the later stages of fire.

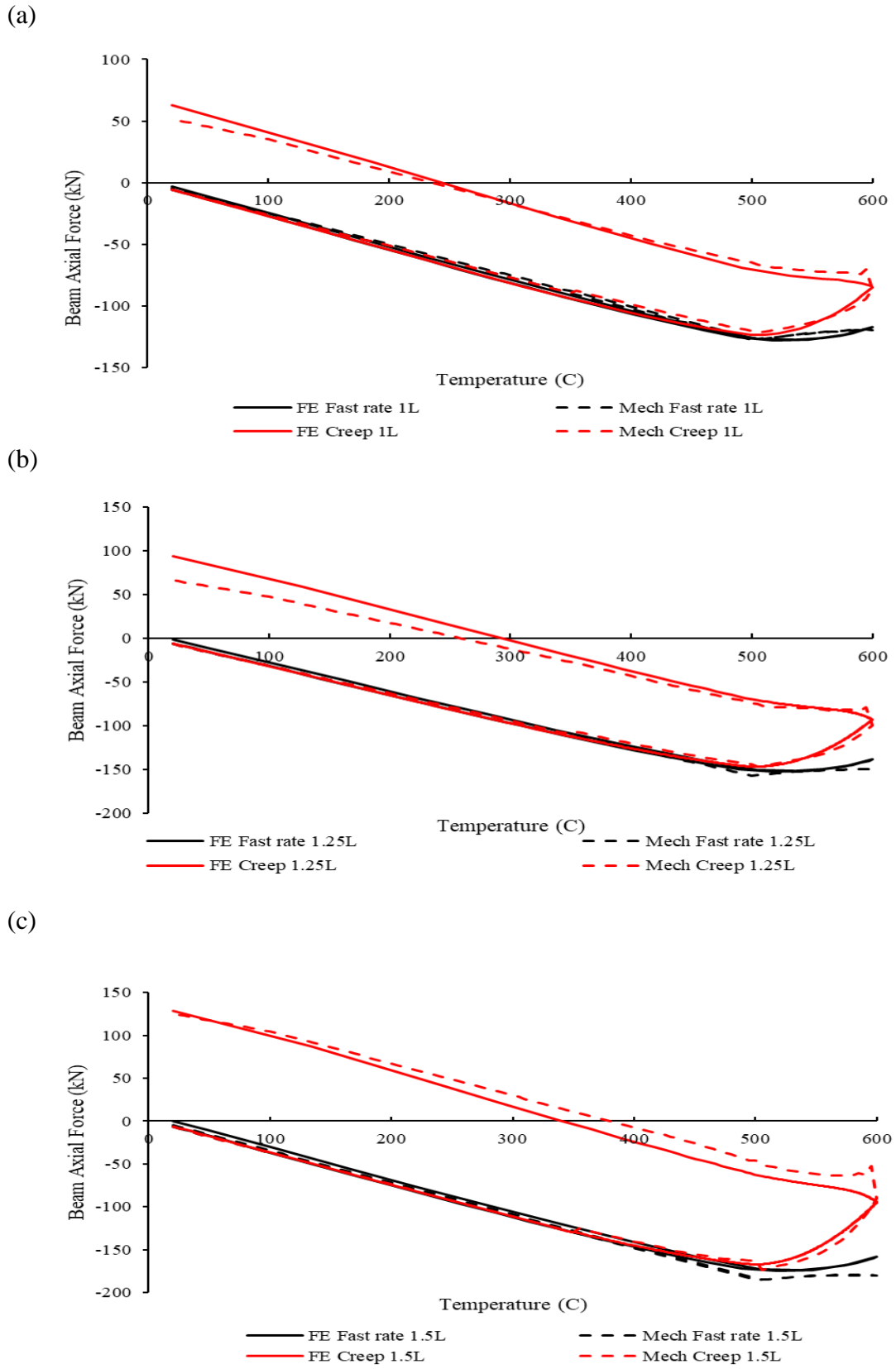
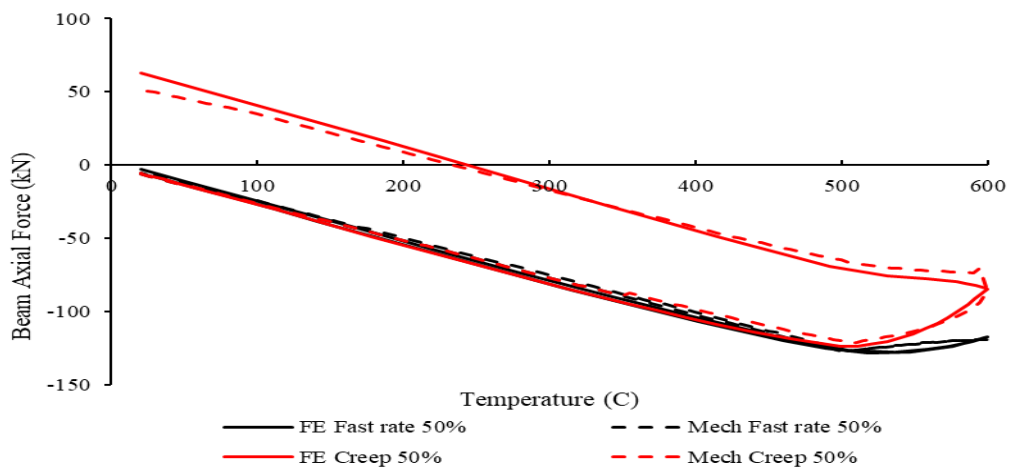


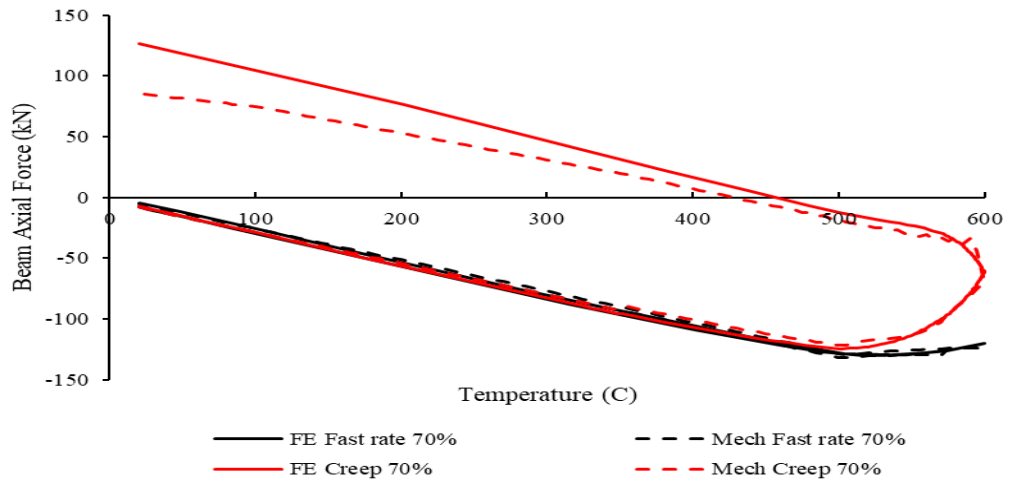
Figure. 16. Mechanical model results on the beam length parameter with and without creep; (a) 1L; (b) 1.25L; (c) 1.5L.

The load ratio is increased from 50% to 70% and 90%, and the results of this parameter are shown in Figure. 17. Also, the model was able to predict the beam axial force with different applied loads with and without the effect of thermal creep strain. When the load ratio reaches 90%, the FE model of the flush end-plate connection showed high stresses along the top bolt row and the top location of the beam web. The failure of the flush end-plate connection is due to a potential end-plate yielding or weld fracture at 575°C. However, the weld fracture cannot be accurately predicted in the FE due to assigning tie constraints at the location of the welds. This failure mode of the connection in the mechanical model was identified as end-plate yielding at 555°C. This shows that the mechanical model also captures the failure mode with reasonable accuracy.

(a)



(b)



(c)

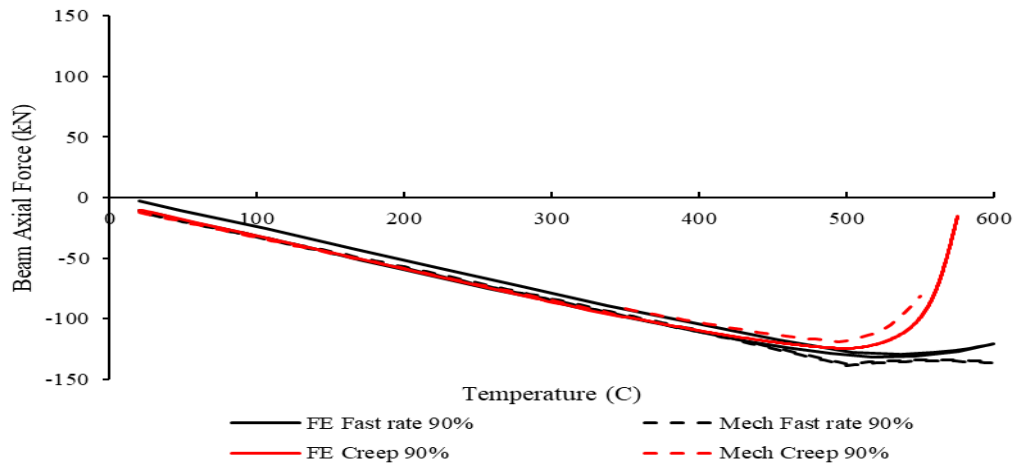


Figure. 17. Mechanical model results on the load ratio parameter with and without creep;

(a) 50%; (b) 70%; (c) 90%.

CHAPTER IV

SUMMARY, CONCLUSIONS AND RECOMMENDATIONS

A. Summary and conclusions

The results of a mechanical model and a series of FE models are presented to understand the behavior of flush end-plate connections in fire. A mechanical model was developed to predict the generated beam axial force in a beam-column flush end-plate connection subjected to fast and prolonged transient heating conditions. The unheated lengths of the column and the thermal creep strains presented challenges in the development of the mechanical model. To overcome these challenges, the lateral stiffness of the unheated column lengths were accounted for in the equivalent connection stiffness. Moreover, the thermal creep strains were included using the *Fields and Fields* thermal creep equation. This mechanical model is developed using an Excel sheet. Once the Excel sheet is written, it becomes simple to analyze the behavior of the connection when studying different parameters.

The FE models were developed in ABAQUS and validated against experimental work found in the literature. Extensive parametric studies were conducted to study their effect on the behavior of the connection with and without thermal creep. The parameters studied were the heating/cooling rate, beam length, load ratio, creep in bolts and flush end-plate thickness and bolt diameter. The creep effect was explicitly incorporated to the heated part of the column, beam, flush-end plate, and bolts. The following can be concluded from this study:

- The mechanical model proved its ability to predict the beam axial force with reasonable accuracy and the connection failure mode. This model captures the different beam axial forces in fast and prolonged fires, as well as in the heating and cooling stages.
- The mechanical, in a straightforward manner, incorporates the thermal creep equation to understand the time-dependent behavior of the flush end-plate connection. While the FE analysis utilizes user-defined subroutines to account for the thermal creep strains of structural steel explicitly.
- The FE models are able to predict the beam axial force and mid-span deflection of the beam-column connection with reasonable accuracy. The FE models also predict the deformed shape and failure mode of the connection.
- The beam axial force and mid-span deflection in the thermal creep models are shown to be dependent on the duration of heating/cooling. It is evident that when the temperature is higher than 500°C, the beam compressive axial force decreases and mid-span deflection increases as the heating/cooling rate decrease.
- The thermal creep effect depends on the heating/cooling rate, beam length, and load ratio. However, the bolt size and the creep effect in bolts have a negligible effect on the time-dependent global response of the connection.

- The effect of thermal creep on the increasing load ratio is reducing the beam compressive axial force at later stages of fire while generating higher tensile forces at the end of the cooling stage.

The FE analysis used in this study produces results with good accuracy, but at the expense of high time consumption and costly computational efforts. Compared to the conventional methods, experimental testing and numerical analysis, mechanical modeling is the most efficient method to understand the behavior of a flush end-plate connection. Furthermore, this method will help engineers study different connections for structural fire engineering applications.

B. Recommendations

Further work should be conducted to fully understand the behavior of flush end-plate connections in fire.

- An FE fracture model is needed to analyze the post-yielding response of the connection in transient fires.
- More experimental work should be performed on full-scale connections in different heating and cooling rates for validation purposes.
- A creep model for welds should be considered in the analysis to be able to fully understand the global behavior of a flush-end plate connection in fire.
- The thermal creep effect should be quantified and studied at temperatures larger than 600°C.
- Research should be conducted on different connections to understand their time-dependent behavior.

Neglecting the effect of thermal creep strains in the analysis of connections in fire may result in unsafe predictions of its behavior. Researchers are quantifying the effect of thermal creep on structures to ensure better fire safety designs in the future.

BIBLIOGRAPHY

- ABAQUS 2014. 6.14 Documentation. *Dassault Systemes Simulia Corporation*, 651.
- AL-JABRI, K. 2004. Component-based model of the behaviour of flexible end-plate connections at elevated temperatures. *Composite structures*, 66, 215-221.
- AL-JABRI, K. S., SEIBI, A. & KARRECH, A. 2006. Modelling of unstiffened flush end-plate bolted connections in fire. *Journal of Constructional Steel Research*, 62, 151-159.
- AL HADDAD, H. O., HANTOUCHE, E. G. & AL KHATIB, K. K. 2019. Numerical Studies on the Creep Behavior of Shear Endplate Connection Assemblies UNDER Transient Heating. *Fire Technology*, 55, 2341-2367.
- BLOCK, F. M., BURGESS, I. W., DAVISON, J. B. & PLANK, R. J. 2007. The development of a component-based connection element for endplate connections in fire. *Fire Safety Journal*, 42, 498-506.
- DAI, X. H., WANG, Y. C. & BAILEY, C. G. 2010. Numerical modelling of structural fire behaviour of restrained steel beam–column assemblies using typical joint types. *Engineering Structures*, 32, 2337-2351.
- DEL SAVIO, A. A., NETHERCOT, D. A., VELLASCO, P. C. G. S., ANDRADE, S. A. L. & MARTHA, L. F. 2009. Generalised component-based model for beam-to-column connections including axial versus moment interaction. *Journal of Constructional Steel Research*, 65, 1876-1895.
- DONG, G., BURGESS, I., DAVISON, B. & SUN, R. 2015. Development of a general component-based connection element for structural fire engineering analysis. *Journal of Structural Fire Engineering*, 6, 247-254.
- EL GHOR, A. H. & HANTOUCHE, E. G. 2017. Thermal creep mechanical-based modeling for flush endplate connections in fire. *Journal of Constructional Steel Research*, 136, 11-23.

- EL KALASH, S. & HANTOUCHE, E. 2017. Mechanical modeling for predicting the axial restraint forces and rotations of steel top and seat angle connections at elevated temperatures. *Journal of Structural Fire Engineering*, 8, 258-286.
- EUROCODE 3-1.2, C. 2005. 1-2, Eurocode 3: Design of steel structures, Part 1.2: General rules–Structural fire design. *Brussels, Belgium: Comité Européen de Normalisation*.
- EUROCODE 3-1.8, C. 2005. 1-8 Eurocode 3: Design of steel structures, Part 1.8: Design of joints. *Brussels: European Committee for Standardization*
- FIELDS, B. & FIELDS, R. 1988. Elevated temperature deformation of structural steel.
- HANTOUCHE, E. G., AL KHATIB, K. K. & MOROVAT, M. A. 2018. Modeling creep of steel under transient temperature conditions of fire. *Fire Safety Journal*, 100, 67-75.
- HU, Y., DAVISON, J., BURGESS, I. & PLANK, R. 2007. Comparative study of the behaviour of BS 4190 and BS EN ISO 4014 bolts in fire. *Proc., ICSCS*, 587-592.
- KODUR, V., DWAIKAT, M. & FIKE, R. 2010. High-Temperature Properties of Steel for Fire Resistance Modeling of Structures. *Journal of Materials in Civil Engineering*, 22, 423-434.
- KODUR, V. K. R. & DWAIKAT, M. M. S. 2010. Effect of high temperature creep on the fire response of restrained steel beams. *Materials and Structures*, 43, 1327-1341.
- LEE, J., MOROVAT, M. A., HU, G., ENGELHARDT, M. D. & TALEFF, E. M. 2013. Experimental investigation of mechanical properties of ASTM A992 steel at elevated temperatures. *Engineering Journal*, 50, 249-272.
- LIE, T. Structural fire protection. 1992. American Society of Civil Engineers.
- MATAR, M. 2014. Primary creep in ASTM A325 bolts under simulated fire loading.
- MOROVAT, M. 2014. High-Temperature Creep Buckling Phenomenon of Steel Columns Subjected to Fire. *Journal of Structural Fire Engineering*, 5, 189-202.

- MOROVAT, M. A., EL GHOR, A. H. & HANTOUCHE, E. G. 2018. Time-dependent response of flush endplate connections to fire temperatures. *Journal of Structural Engineering*, 144, 04018023.
- MURRAY, T. & SHOEMAKER, W. 2002. Flush and Extended Multiple-Row Moment End-Plate Connections (Steel Design Guide 16). American Institute of Steel Construction, USA.
- NIST, N. 2008. 1A: Final Report on the Collapse of World Trade Center Building 7. *National Institute of Standards Technology, Gaithersburg, USA*.
- POH, K. 2001. Stress-strain-temperature relationship for structural steel. *Journal of materials in civil engineering*, 13, 371-379.
- QIANG, X., BIJLAARD, F., KOLSTEIN, H. & TWILT, L. 2013. Numerical analysis of high strength steel endplate connections at ambient and elevated temperatures. *Journal of Structural Fire Engineering*, 4, 143-152.
- SILVA DA, L. S., SANTIAGO, A., REAL, P. V. & MOORE, D. 2005. Behaviour of steel joints under fire loading. *Steel and Composite Structures*, 5, 485-513.
- TORIC, N., SUN RUI, R. & BURGESS IAN, W. 2016. Creep-free fire analysis of steel structures with Eurocode 3 material model. *Journal of Structural Fire Engineering*, 7, 234-248.
- WANG, W., YAN, S. & LIU, J. 2016. Studies on temperature induced creep in high strength Q460 steel. *Materials and Structures*, 50, 68.
- WANG, Y. C., DAI, X. H. & BAILEY, C. G. 2011. An experimental study of relative structural fire behaviour and robustness of different types of steel joint in restrained steel frames. *Journal of Constructional Steel Research*, 67, 1149-1163.
- YU, H., BURGESS, I. W., DAVISON, J. B. & PLANK, R. J. 2011. Experimental and Numerical Investigations of the Behavior of Flush End Plate Connections at Elevated Temperatures. *Journal of Structural Engineering*, 137, 80-87.
- YU, H. X. & LIEW, J. Y. R. 2005. Considering Catenary Action in Designing End-Restrained Steel Beams in Fire. *Advances in Structural Engineering*, 8, 309-324.

APPENDIX

Below is the user-defined subroutine used in this paper to account for the thermal creep strains of the structural steel and bolts. The subroutine was previously proposed by Hantouche et al. (2018) and Al Haddad et al. (2019) and then further developed in this study to include the thermal creep strains of bolts.

```
SUBROUTINE CREEP (DECRA, DESWA, STATEV, SERD, EC, ESW, P, QTILD,  
1 TEMP, DTEMP, PREDEF, DPRED, TIME, DTIME, CMNAME, LEXIMP, LEND,  
2 COORDS, NSTATV, NOEL, NPT, LAYER, KSPT, KSTEP, KINC)  
C  
C INCLUDE 'ABA_PARAM.INC'  
C  
C CHARACTER*80 CMNAME  
C  
C DIMENSION DECRA(5), DESWA(5), STATEV(*), PREDEF(*), DPRED(*),  
1 TIME(3), COORDS(*), EC(2), ESW(2)  
C  
C DEFINE CONSTANTS  
XN = 2.1+0.0064*TEMP  
XM = -1.1+0.0035*TEMP-1  
IF (TEMP<=450.AND.CMNAME(1:12).EQ."Column Bolts") THEN  
XD = 0  
XE = 1  
XF = 1  
XG = 1  
END IF  
IF (TEMP>450.AND.TEMP<=500.AND.CMNAME(1:12).EQ."Column  
Bolts") THEN  
XD = -3.97346*(10**-06)*TEMP+1.987057*(10**-03)  
XE = 1.264752*(10**-2)*TEMP-5.468964  
XF = -4.88282502*TEMP+2443.778  
XG = 2.9734*(10**-3)*TEMP-1.2668  
END IF  
IF (TEMP>500.AND.CMNAME(1:12).EQ."Column Bolts") THEN  
XD = -1.72*(10**-9)*TEMP+1.187*(10**-06)  
XE = -6.688*(10**-04)*TEMP+1.189196  
XF = 0.14191654*TEMP-68.593121  
XG = 5.2552*(10**-3)*TEMP-2.40758  
END IF  
C2=1./XG  
IF (LEXIMP.EQ.0) THEN  
EC0=EC(1)  
TERM1=(XD*C2*exp(-XF/TEMP)*(145038*QTILD)**XE)**C2  
TERM2=TERM1*DTIME*60+EC0**C2  
DECRA(1)=(TERM2**XG)-EC0
```

END IF

C

```
IF (LEXIMP.EQ.1) THEN  
  EC0=EC(1)  
  TERM1=(XD*C2*exp(-XF/TEMP)*(145038*QTILD)**XE)**C2  
  TERM2=TERM1*DTIME*60+EC0**C2  
  DECRA(1)=(TERM2**XG)-EC0  
  DECRA(5)=DTIME*60*XE*(1/(145038*QTILD))*TERM1*TERM2**(XG-1)  
END IF
```

C

```
IF (TEMP<=350) THEN  
  A = 0  
  XN = 1  
  XM = 1  
END IF  
IF (TEMP<500.AND.TEMP>350.AND.CMNAME(1:11).NE."Long column")  
THEN  
  A =(10**(-6.1-0.00573*TEMP)/100)*(145.03774**XN)*(XM+1)  
END IF  
IF (TEMP>=500.AND.CMNAME(1:11).NE."Long column") THEN  
  A=(10**(0.00851*TEMP-13.25)/100)*(145.03774**XN)*(XM+1)  
END IF  
IF (CMNAME(1:11).EQ."Long column".AND.TEMP<500.AND.TEMP>350)  
THEN  
  A =(10**(-6.1-0.00573*TEMP)/100)*(145.03774**XN)*(XM+1)*0.72**XN  
END IF  
IF (CMNAME(1:11).EQ."Long column".AND.TEMP>=500) THEN  
  A=(10**(0.00851*TEMP-13.25)/100)*(145.03774**XN)*(XM+1)*0.72**XN  
END IF  
  C1=1./(1.+XM)  
IF(LEXIMP.EQ.0) THEN  
  EC0=EC(1)
```